water

MDPI

Article

Convective Precipitation Fractions and Water Isotopes: A Multi-Dataset Assessment Across Six European Stations

Elemér László [1,*], Mátyás Baksa [1,2], László Palcsu [1], Ádám Vas [3], Mariana Souza Sampaio [1,4], Ádám Leelőssy [5] and Danny Vargas [1]

1 Isotope Climatology and Environmental Research Group (ICER), HUN-REN Institute for Nuclear Research, (ATOMKI), Bem tér 18/C, H-4026 Debrecen, Hungary; baksa.matyas@atomki.hu (M.B.); palcsu.laszlo@atomki.hu (L.P.); danny.vargas@atomki.hu (D.V.)
2 Doctoral School of Physics, University of Debrecen, H-4026 Debrecen, Hungary
3 Department of Informatics Systems and Networks, Faculty of Informatics, University of Debrecen, Kassai út 26, H-4028 Debrecen, Hungary; vas.adam@inf.unideb.hu
4 Institute of Earth Sciences, Faculty of Science and Technology, University of Debrecen, Egyetem tér 1, H-4010 Debrecen, Hungary
5 Department of Meteorology, Institute of Geography and Earth Sciences, Eötvös Loránd University, Pázmány Péter sétány 1/A, H-1117 Budapest, Hungary; adam.leelossy@ttk.elte.hu
* Correspondence: laszlo.elemer@atomki.hu

Abstract

The stable (δ^2H, δ^{18}O) and radioactive (^{3}H) isotopic signals in precipitation are important hydrological tracers and key elements for understanding the water circulation on Earth. Variations in the water isotopic composition at midlatitudes have been classically studied as closely dependent on temperature. In recent years, the concept of temperature control has been refined, and new findings indicate that convective and stratiform precipitation might play a fundamental role in their isotopic fractionation, particularly at the tropics. At midlatitudes, especially in Central Europe, little is known regarding the existence of this relationship. This study addresses the problem by harnessing the monthly δ^2H, δ^{18}O, and ^{3}H records (2000–2018) from six Central European stations across the Carpathian Basin and northward. We segregate the type of precipitation into stratiform, convective, and mixed using SYNOP report data and use this information to clarify the relationships observed between rainwater tracers, focusing on the δ^{18}O-^{3}H correlation and the deuterium excess (d-excess) during summertime. We investigate whether the seasonal occurrence of convective and stratiform precipitation is associated with variations in precipitation δ^{18}O, δ^2H, ^{3}H and d-excess. Our results show that the seasonal increase in convective precipitation coincides with higher δ^{18}O and ^{3}H values at the investigated stations, although tritium associations are not significant after seasonal adjustment, and additional explanatory contributions for stable isotopes are modest and station-dependent.

Keywords: stable isotopes; oxygen-18; tritium; deuterium excess; SYNOP; convective precipitation; stratiform precipitation; mixed precipitation; GPM

Check for updates

Academic Editors: Fengtian Yang and Xiaodong He

Received: 10 October 2026
Revised: 19 November 2026
Accepted: 24 November 2026
Published: 27 November 2026

Copyright: © 2026 by the authors. Licensee MDPI, Basel, Switzerland. This article is an open access article distributed under the terms and conditions of the Creative Commons Attribution (CC BY) license.

1. Introduction

Understanding the processes controlling the isotopic composition of precipitation is important for interpreting the hydrological cycle and for improving the representation of atmospheric moisture processes in climate and hydrological models. Stable water isotopes (δ^{18}O and δ^2H) and radioactive tritium (^{3}H) have long been used as tracers of atmospheric and terrestrial water circulation. Their variability in precipitation reflects the combined

effects of moisture source conditions, atmospheric transport, condensation history, precipitation formation, and post-condensation processes.

The large-scale controls on stable isotope variability in precipitation differ geographically and seasonally. In tropical regions, $\delta^{18}O$ and $\delta^{2}H$ are often related to precipitation amount and to the organization and history of atmospheric convection, whereas at mid- and high latitudes their seasonal variability is strongly associated with air temperature [1–4]. In Europe, precipitation is generally more depleted in $\delta^{18}O$ and $\delta^{2}H$ during winter and more enriched during summer [1,2,4,5].

However, temperature alone cannot account for all precipitation isotope variability because the measured isotope composition integrates processes occurring throughout the atmospheric history of the moisture, including source conditions, transport, mixing, condensation, and evaporation. This distinction is particularly important when seasonal variations in temperature coincide with systematic changes in atmospheric circulation and precipitation regime.

Additional information on these processes can be obtained from deuterium excess, defined as d-excess = $\delta^{2}H - 8 \times \delta^{18}O$. Deuterium excess describes deviations from the Global Meteoric Water Line and is sensitive to kinetic isotope effects. It can contain information on conditions at the moisture source, particularly relative humidity, but may subsequently evolve during atmospheric transport and precipitation formation [3,4]. Consequently, precipitation d-excess should not be interpreted as a unique indicator of moisture source conditions. Local and regional processes, including sub-cloud evaporation, continental moisture recycling, and seeder–feeder interactions, can modify the d-excess signal during atmospheric transport or before precipitation reaches the surface [6,7]. In particular, sub-cloud evaporation of falling raindrops can decrease precipitation d-excess, whereas continental moisture recycling may have an opposite effect. Thus, d-excess provides information complementary to $\delta^{18}O$ and $\delta^{2}H$ when evaluating possible source-, transport-, and post-condensation effects.

Tritium provides an additional constraint on atmospheric moisture history. Tritium occurs in atmospheric water primarily as HTO and, once incorporated into tropospheric water vapor, participates in the atmospheric water cycle together with the stable water isotopologues. Unlike $\delta^{18}O$ and $\delta^{2}H$, the atmospheric distribution of ^{3}H is additionally influenced by its production history and by exchange and transport between atmospheric reservoirs [8,9]. Natural tritium is produced by interactions of cosmic radiation with atmospheric constituents, while the present atmospheric inventory also reflects the legacy of anthropogenic tritium released during the period of atmospheric thermonuclear testing. Precipitation ^{3}H consequently exhibits pronounced spatial and seasonal variability, including the characteristic spring and early-summer increase observed at many continental Northern Hemisphere stations [10–14].

Once HTO is incorporated into tropospheric water vapor, its concentration in precipitation reflects the tritium content of the contributing atmospheric moisture together with its transport and mixing history. Therefore, covariation between precipitation ^{3}H and stable isotope ratios should not be interpreted as evidence that the same atmospheric or microphysical process controls both tracers. Common seasonality and atmospheric transport may contribute to their covariation, while $\delta^{18}O$, $\delta^{2}H$, and d-excess are additionally modified by equilibrium and kinetic fractionation during condensation, evaporation, and other precipitation-related processes. In this context, ^{3}H and the stable isotope tracers provide complementary rather than interchangeable information about atmospheric moisture history. This distinction is particularly relevant when evaluating whether an observed relationship between tritium activity and convective precipitation reflects an independent association or primarily the coincidence of their seasonal cycles.

An additional source of isotope variability is the physical regime in which precipitation develops. Precipitation can broadly be separated into convective and stratiform components according to differences in cloud dynamics and microphysical growth processes [13]. Convective precipitation is associated with active cumulus and cumulonimbus clouds characterized by strong vertical motions, whereas stratiform precipitation develops under weaker and more widespread vertical motions. Convective and stratiform precipitation may also coexist within the same organized precipitation system. Their distinction therefore represents different precipitation regimes and associated dynamical and microphysical conditions rather than completely independent atmospheric moisture sources. Moreover, the estimated contribution of convective precipitation may depend on whether precipitation regimes are identified from surface weather observations, atmospheric reanalysis products, or satellite-based retrievals. These approaches do not necessarily characterize identical aspects of precipitation organization, and differences between them may affect the interpretation of precipitation-type–isotope relationships.

The relationship between precipitation type and isotope composition has previously been investigated [14]. By combining precipitation isotope observations with convective and stratiform precipitation fractions, the authors identified systematic relationships between rain-type proportions and both stable isotope ratios and ^{3}H. Their interpretation associated higher stable isotope ratios under convective conditions with processes involving boundary-layer moisture, including condensation and riming, whereas enhanced tritium during deep convection was related to interactions with air entrained at higher atmospheric levels. These results demonstrate that precipitation type can contain information on atmospheric processes associated with isotope variability. However, a statistical relationship between precipitation type and isotope composition does not by itself demonstrate that precipitation type directly controls the isotopic signal. In particular, the extent to which such relationships remain detectable after removing the seasonal cycle and accounting for other meteorological influences requires further investigation at midlatitudes.

This distinction is particularly important at midlatitudes. In Central Europe, precipitation regime, temperature, atmospheric circulation, and precipitation isotope composition all exhibit pronounced seasonal variability. Convective precipitation becomes more frequent during the warm season, when δ^{18}O and δ^{2}H values are also generally higher. Precipitation ^{3}H likewise exhibits a strong seasonal cycle. Consequently, a positive correlation between the proportion of convective precipitation and isotope values may arise, at least partly, because both variables covary with season. Conversely, precipitation-related processes may also contribute to differences in stable isotope composition between individual events or precipitation regimes. The effects of common seasonality and process-specific isotope modification therefore need to be distinguished when interpreting precipitation-type–isotope relationships. Comparing correlations calculated from the original monthly observations with those obtained from calendar-month anomalies provides a direct assessment of the influence of the recurring seasonal cycle. However, correlations based on deseasonalized observations may still reflect covariation with temperature, precipitation amount, atmospheric circulation, or other meteorological factors. Multivariable analyses are therefore needed to evaluate whether the convective precipitation fraction provides additional explanatory information beyond these covariates.

Sub-cloud evaporation is one process that may modify the stable isotope composition after condensation. Falling raindrops entering subsaturated air can partially evaporate and undergo kinetic isotope fractionation before reaching the surface. This process can alter δ^{18}O, δ^{2}H, and particularly their relationship expressed by d-excess [7,15]. Its magnitude depends on below-cloud atmospheric conditions and should therefore be regarded as a post-condensation process rather than an intrinsic characteristic of convective precipitation.

Convective precipitation may occur under environmental conditions favorable for sub-cloud evaporation, particularly during warm-season events with relatively dry sub-cloud air, but the occurrence of convection alone does not demonstrate that evaporation has modified the isotope composition of precipitation. Accordingly, the interpretation of d-excess variations benefits from considering atmospheric humidity and temperature alongside precipitation-type information, rather than attributing isotope changes to convection alone.

The present study builds on the precipitation-type framework ofAggarwal et al. (2016) [14]. by examining relationships between precipitation regimes and multiple isotope tracers across six Central European stations: Debrecen (Hungary), Vienna (Austria), Krakow (Poland), Zagreb (Croatia), Cuxhaven (Germany), and Wasserkuppe (Germany). Continuous monthly $\delta^{18}O$, $\delta^{2}H$, and ^{3}H records covering 2000–2024 are combined with precipitation-type information derived from SYNOP reports. Unlike the binary distinction between convective and stratiform precipitation, we explicitly include mixed precipitation as a third category, representing events in which both precipitation processes coexist. This extension allows a more detailed characterization of precipitation regimes and their relationships with isotope composition across contrasting Central European climatic settings.

To assess the sensitivity of the results to precipitation classification, we distinguish between the fraction assigned exclusively to convective precipitation and an alternative definition that also includes the mixed category. We additionally compare these observation-based estimates with convective precipitation fractions derived from ERA5 reanalysis and GPM satellite observations, where suitable overlapping data are available. These comparisons are conducted using both the available source-specific monthly records and matched observation periods to avoid attributing differences caused by unequal temporal coverage to the precipitation datasets themselves.

In addition to the long-term monthly records, higher-frequency isotope observations from Debrecen are used to investigate stable-isotope modifications that cannot be resolved from monthly averages alone. Atmospheric back trajectories are further considered to explore variations in moisture provenance and transport history.

The first objective of this study is to quantify the association between the seasonal occurrence of convective, stratiform, and mixed precipitation and variations in $\delta^{18}O$, $\delta^{2}H$, and ^{3}H across the six stations. Because precipitation type and isotope composition both exhibit pronounced seasonal cycles, these associations are not interpreted as direct evidence of causality. Instead, we assess whether precipitation-type proportions provide additional information for interpreting the observed seasonal isotope variability.

Specifically, we evaluate the extent to which precipitation-type–isotope relationships persist after removal of the mean annual cycle and whether the strength of these relationships depends on the method used to estimate convective precipitation fraction. We further examine the contribution of convective precipitation fraction within multiple regression models that account for selected meteorological covariates. Statistical inference is evaluated with methods designed to address temporal dependence and multiple testing, while the relative explanatory contributions of model predictors are examined separately from their statistical significance.

The second objective is to examine d-excess together with the higher-resolution Debrecen isotope observations to assess whether post-condensation processes, particularly sub-cloud evaporation, contribute to the stable-isotope variability. Finally, atmospheric back trajectories are used to explore whether differences in moisture provenance and transport history are associated with the observed variations in precipitation isotope composition.

We hypothesize that precipitation-type proportions covary with isotope composition at the investigated Central European stations, but that this relationship reflects the combined effects of seasonality, atmospheric moisture transport, and precipitation-related processes

rather than direct control by convection alone. We use $\delta^{18}O$, $\delta^{2}H$, and d-excess to assess stable-isotope modifications associated with precipitation and below-cloud processes, while interpreting variations in precipitation ^{3}H in terms of the tritium content and transport history of atmospheric moisture. By distinguishing statistical association from process attribution, this framework identifies which aspects of isotope variability can be resolved from long-term monthly observations and which require higher-frequency isotope and meteorological data.

We further hypothesize that the apparent relationship between convective precipitation fraction and isotope composition will differ among isotope tracers after seasonal adjustment, reflecting their distinct sensitivities to atmospheric processes. In particular, we expect the interpretation of tritium–convection relationships to require greater consideration of shared seasonality and moisture transport than is possible from unadjusted correlations alone. By combining alternative precipitation classifications, deseasonalized correlations, and multivariable statistical analyses, the study aims to establish a more robust basis for evaluating the information provided by precipitation regime about midlatitude precipitation isotope variability.

2. Materials and Methods

2.1. Climatic Characteristics of the Stations

The six meteorological stations analyzed in this paper were Debrecen, Vienna, Krakow, Zagreb, Cuxhaven, and Wasserkuppe, as presented in Figure 1. They were chosen to better represent the diversity of climates in Central Europe, the quality of the continuous monitoring of $\delta^{2}H$, $\delta^{18}O$, and ^{3}H and to capture inland moisture variability in the region. The first meteorological station is situated in Debrecen (47.5° N, 21.5° E), with WMO station number 12882. It is a nearly flat region that lies at a height of 110 m.a.sl. in the Great Hungarian Plain. According to Köppen's climate classification, the city belongs to the climate region Cfb (temperate warm-summer climate [16]. With moist summers and drier winters, the mean monthly precipitation amount varies from 28 mm in January to 76 mm in July, and the annual average precipitation is 554 mm. The mean temperature is 11.1 °C, with monthly averages from −0.8 °C to 22.0 °C throughout the year.

The Vienna station (48.2° N, 16.4° E), with WMO station number 11035, is located in the Vienna Basin at 198 m.a.s.l. The mean annual temperature is 11.24 °C, varying from 0.8 °C to 21.7 °C, and the summer is the moistest season. April is the driest month, with a mean precipitation of 36.5 mm, while 85 mm can be observed in May, the moistest month. The annual mean precipitation for the station is 673 mm. Vienna also has a temperate warm-summer climate, categorized as Cfb by Köppen's climate classification.

The Krakow station (50.1° N, 19.9° E), with WMO station number 12565, is located in the Vistula River valley, near the northern edge of the Carpathian Mountains, at 205 m.a.s.l. The mean temperatures range from −2.0 °C in January to 19.6 °C in July, with an annual mean of 9.0 °C, and the highest mean precipitation amounts can be observed in the warmest months, varying from 32 mm to 90 mm. The annual amount of precipitation in the city is 663 mm.

Zagreb (45.8° N, 16.0° E), with WMO station number 13127 for the Gric station, also belongs to the Cfb climate zone, but it is located on the border with the humid subtropical climate region (Cfa), presenting strong Mediterranean influences. The station has an elevation of 157 m.a.s.l. Zagreb records the highest mean temperatures among the analyzed stations, with an annual mean of 13.1 °C, ranging between 2.5 °C and 23.5 °C monthly means. The mean annual precipitation is 871 mm. September is the moistest month with a mean precipitation amount of 108 mm, whereas December is the driest month with only 52 mm.

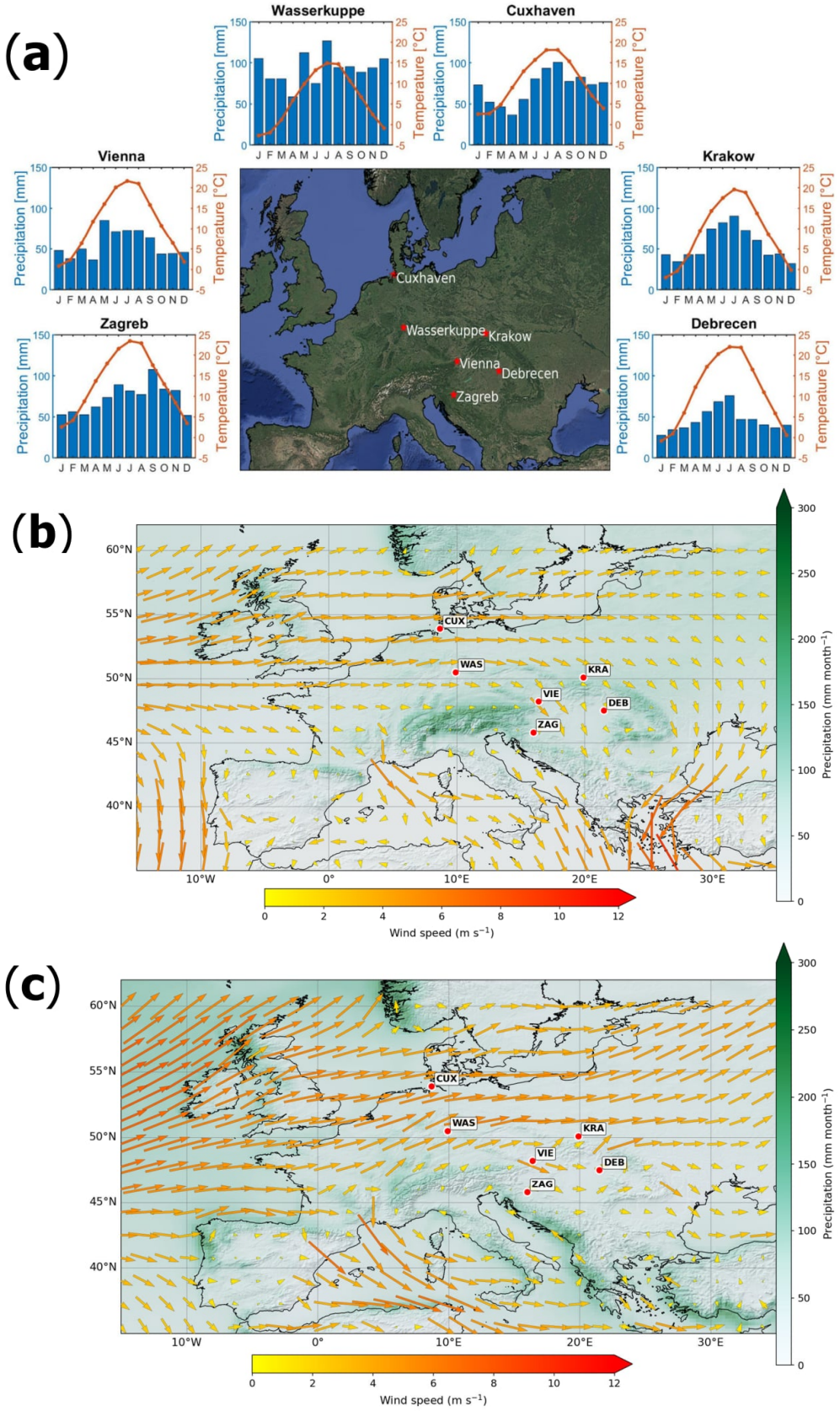

Figure 1. Climatological characteristics of the studied stations: Debrecen (HU), Vienna (AT), Krakow (PL), Zagreb (HR), Cuxhaven (DE) and Wasserkuppe (DE). (**a**) Annual temperature (orange line) and precipitation (blue bars) from 2000 to 2018. (**b**) ERA5 precipitation and 925 hPa (~750 m a.s.l.) mean westerly winds (1940–2025) for summer (JJA) and (**c**) winter (DJF).

Also part of the Cfb climate region, Cuxhaven (53.9° N, 8.7° E), with WMO station number 10131, is located on the coast of Germany (12 m.a.s.l.). Its climate is strongly influenced by the Atlantic Ocean. The monthly mean temperatures range from 2.6 °C to 18.1 °C, with a 10.1 °C annual mean. The warmest months are also the moistest, with the mean monthly precipitation amount reaching 100 mm in August. The monthly mean is lowest in April, with only 37 mm of precipitation. The city presents an annual average precipitation of 849 mm.

Finally, Wasserkuppe (50.5° N, 9.9° E), with WMO station number 10544, is the sixth meteorological station analyzed in this paper, presenting a temperate climatic zone and high altitude. With an elevation of 921 m.a.s.l., it is the highest peak in the Rhön Mountains. The region has the lowest temperatures among the studied stations, with an annual average of 6.2 °C and monthly means varying from −2.7 °C to 14.9 °C. The region receives the highest annual mean precipitation amount among the analyzed stations: 1116 mm per year, ranging from 59 mm in April to 127 mm in July.

2.2. SYNOP Reports and Statistics

Recent approaches for distinguishing convective and stratiform precipitation commonly use ground-based weather radar and satellite observations. Radar-based classification methods exploit differences in the spatial and vertical structure of reflectivity associated with the contrasting dynamical and microphysical characteristics of convective and stratiform precipitation [13]. Convective precipitation is generally associated with stronger vertical motions and localized regions of enhanced reflectivity, whereas stratiform precipitation is characterized by weaker and more widespread vertical motions and may exhibit a melting-layer bright band. Radar and satellite observations can also provide spatially distributed estimates of precipitation intensity and amount. However, surface observations provide long-term, station-specific information on precipitation occurrence and type, including present-weather codes that can be used to distinguish precipitation regimes [17].

In the present study, precipitation type was classified using long-term surface synoptic observations (SYNOP), which provide a consistent station-based record for the six investigated sites over the study period. A SYNOP-based algorithm was applied to distinguish convective, stratiform, and mixed precipitation regimes using present-weather, past-weather, and cloud-type observations. The SYNOP reports were obtained from the OGIMET website, a weather information service that uses freely available meteorological data from instrumental stations.

The current weather is presented in SYNOP reports using two-digit present-weather codes (ww). Codes from 00 to 49 generally describe weather conditions without precipitation occurring at the station at the observation time, whereas codes from 50 to 99 describe precipitation-related phenomena. Each number represents a specific weather phenomenon, such as thunderstorms, drizzle, or rain showers. Additional convective indicators (codes 17–19 and 25–29), past-weather codes, and cloud-type observations were also considered in the classification.

The classification algorithm was applied to six-hour precipitation intervals rather than entire days, using precipitation amounts reported in SYNOPs. The algorithm distinguished four categories (Supplementary Materials Figure S1): Category 0 represented intervals without precipitation; Category 1 included convective precipitation, such as rain showers and thunderstorms; Category 2 included stratiform precipitation, such as continuous rain, snow, and drizzle; and Category 3 represented mixed precipitation. Intervals with insufficient or ambiguous evidence were retained as a separate unclassified category. Three classification variants (strict, maximum, and final), adapted from the framework of Rulfová and Kyselý (2013) [17], were implemented to assess classification sensitivity.

To restrict the analysis to actual precipitation events, records with less than 0.1 mm of precipitation were excluded from the precipitation-type fraction calculations. Unusually high precipitation values, potentially indicating erroneous observations, were cross-checked against the corresponding weather reports available from OGIMET for the respective station and date. Additional quality-control procedures included checks for conflicting precipitation records and consistency between six-hour, twelve-hour, and available daily precipitation totals. Missing six-hour precipitation amounts could be reconstructed from overlapping twelve-hour accumulations only when a valid twelve-hour total and exactly one valid six-hour amount were available for the same twelve-hour interval. The missing amount was calculated as the difference between these two observations. Conflicting observations differing by more than 0.1 mm and reconstructed values yielding negative residuals beyond the 0.1 mm tolerance were rejected. Small negative residuals within this tolerance were set to zero. Reconstructed values were flagged separately. Monthly precipitation-type fractions were calculated from the precipitation amounts assigned to each category, rather than from event frequencies alone.

The SYNOP-based classification results were compared with those obtained from the Global Precipitation Measurement (GPM) Gridded Convective–Stratiform Heating (3GCSH) dataset [18–20]. The 3GCSH algorithm relies on space-based radar measurements, providing estimates of latent heating associated with convective and stratiform precipitation regions. The GPM data are available at a spatial resolution of 0.5° × 0.5° and a temporal resolution of 1.5 h. The convective precipitation fraction was calculated as the complement of the stratiform fraction (CPF = 1 − stratiform fraction), considering only observations for which precipitation intensity data were available. Monthly convective precipitation fractions were subsequently derived from these valid observations and compared with SYNOP- and ERA5-based estimates over their common observation period (2014–2024). Agreement was assessed using mean bias, root mean square error (RMSE), and Pearson's correlation coefficient (Table S1).

2.3. Gridded Products

We extracted gridded products from the ERA5 and CHELSA databases. We focused on the extraction of datasets closely related to and comparable with SYNOP convective precipitation. For ERA5, we obtained the values from the post-processed daily statistics on single levels from 2000 to 2024 [20]; available at https://cds.climate.copernicus.eu/datasets/derived-era5-single-levels-daily-statistics (accessed on 23 November 2026). The retrieved products were convective available potential energy (CAPE; J kg^{-1}), cloud base height (CBH; m), and boundary layer height (BLH; m).

In addition, ERA5 convective and total precipitation fields were used to calculate the monthly convective precipitation fraction. The fraction was defined as the ratio of accumulated convective precipitation to accumulated total precipitation over the corresponding month, expressed as a percentage (CPF_ERA5 = 100 × P_conv/P_total), where P_conv and P_total represent monthly accumulated convective and total precipitation, respectively. Months without positive total precipitation were excluded from this calculation. ERA5-based CPF estimates were compared with the SYNOP-derived fractions and GPM-based estimates during their overlapping observation periods.

In addition, we complement our dataset with the extraction of the moisture index from the CHELSA product [21] (https://web.archive.org/web/20250817055722/https://chelsa-climate.org/timeseries/ (accessed on 23 November 2026)). The CHELSA moisture index is defined as the difference between monthly precipitation and monthly potential evapotranspiration. The retrieved meteorological data was summarized employing seasonal boxplots (Supplementary Materials Figure S13).

2.4. Water Isotopes Dataset and Analytical Measurements

This study uses quantitative data for δ^2H, $\delta^{18}O$ and ^3H gathered from different sources for the 2000–2022 period. The list includes the IAEA/GNIP database, published articles [22–25], and measurements made in institutes and universities (Institute of Physics, AGH Krakow; Deutscher Wetterdienst; Helmholtz-Zentrum, München; BAFG, Koblenz; Ruder Boskovic Institute, Zagreb [26,27]). In the case of the Debrecen samples, the measurements were carried out by the HUN-REN Institute for Nuclear Research (ATOMKI). Some datasets were obtained from the GNIP database, while others were derived from our own measurements or compiled from previously published studies. These datasets were combined to provide a more representative characterization of the isotopic composition at each station over the analyzed period. Quality control was carried out on the datasets where gaps were found. The temporal coverage and completeness of the monthly precipitation isotope datasets varied among the six monitoring stations (Table S2). Stable isotope observations covered periods ranging from 2000 to 2012 at Cuxhaven to 2000–2022 at Vienna, whereas tritium records extended to 2021 or 2022 at several stations. The number of valid paired monthly $\delta^{18}O$ and δ^2H observations used to calculate the Local Meteoric Water Lines (LMWLs) ranged from 156 at Cuxhaven to 266 at Vienna. The availability of simultaneous $\delta^{18}O$, δ^2H, and ^3H measurements also differed among stations, with 156–259 complete monthly isotope records. Missing observations were excluded from the analyses without interpolation. Detailed information on station-specific observation periods, sample sizes, and isotope data coverage is provided in Supplementary Table S3.

The measurements for Debrecen were performed using a Los Gatos Research Liquid Water Isotope Analyzer (LGR LWIA-24i, ABB-Los Gatos Research, San Jose, CA, USA) during the period 2015–2018. The samples from the first 14 years were analyzed using an Isotope Ratio Mass Spectrometer (IRMS). The internal laboratory standards were calibrated against international water standards, V-SMOW, GISP, and SLAP [24]. The reproducibility was better than 0.16‰ for $\delta^{18}O$ and better than 1.04‰ for δ^2H, based on replicates of laboratory standards. Evaluation of the measurements employed the Liquid Water Isotope Analyzer Post Processor, which loads all the data, performs the required standardization and processing steps, and exports the processed data to a text file.

It is noteworthy to mention that, as the δ^2H and $\delta^{18}O$ values were highly correlated for all the stations and do not present significant deviations from the global and local Meteoric Water Lines (GMWL and LMWL, respectively), the subsequent sections will only refer to $\delta^{18}O$, as the obtained results will be similar if δ^2H was used. In addition, the investigation of δ^2H was indirectly employed through the d-excess values. The characteristics of the Local Meteoric Water Lines (LMWLs) calculated for each station provide important insights into the atmospheric processes shaping precipitation. In this study, daily and monthly precipitation isotope data were used for Debrecen, while monthly averaged data were employed for other European stations (Vienna, Krakow, Zagreb, Cuxhaven, Wasserkuppe). For Debrecen, daily precipitation isotope observations from two periods (2000–2009 and 2015–2018) were additionally used for event-level analyses. These observations were analyzed separately from the monthly datasets used for the six-station comparisons and were matched with meteorological variables derived from ERA5 over the corresponding precipitation sampling intervals. The event selection criteria, matching procedure, and statistical treatment are described in Section 2.6. Finally, the ^3H measurements were performed at the Noble Gas Laboratory of HUN-REN ATOMKI, Debrecen, Hungary, using the ^3He ingrowth method as described in previous studies [28,29]. The ^3H activities were expressed in tritium units (TU), where 1 TU represents a $^3H/^1H$ ratio of 1×10^{-18}. The analytical uncertainties of the ^3H measurements were reported as one standard deviation (1σ), expressed in tritium units (TU). The mean 1σ uncertainties ranged from 0.23 TU at Debrecen to 1.35 TU at Cuxhaven.

The corresponding values were 0.60 TU for Krakow, 0.38 TU for Zagreb, 0.44 TU for Vienna, and 1.27 TU for Wasserkuppe. Across all six stations, individual 1σ uncertainties ranged from 0.04 to 2.85 TU. Station-specific mean, minimum, and maximum uncertainties are summarized in Supplementary Table S2.

2.5. Backtrajectories and Moisture Provenance

We used the HYSPLIT (HYbrid Single-Parcel Lagrangian Integrated Trajectory) model [30–32] in a scripted workflow via the PySPLIT python package [33,34] to run backward trajectories for all the European stations. The bulk trajectories were calculated 5 days backwards (−120 h) from 2005 to 2018 (14 years) at four different levels: 500, 1500, 3000, and 5000 m ASL, every second day of the month and two times per day (00 and 12 h) (Supplementary Figures S4–S7). The GDAS (Global Data Assimilation System) at 1° × 1° spatial and 3 h time resolution was used as the input meteorology. From the generated bulk of trajectories for all the stations, we performed cluster analysis programmatically through the Openair R package [35] (https://openair-project.github.io/book/ (accessed on 23 November 2026)) to post-process and group similar air mass origins together. The back-trajectories were grouped by seasons (DJF, MAM, JJA, SON) in five clusters, employing the angle-based measure for the matrix distance calculation, which aggregates similar trajectories in terms of their angle from the origin and captures relevant atmospheric circulatory features. In addition, we utilized the geographical coordinates of the generated cluster trajectories as input to extract the monthly mean d-excess value from the isoscapes gridded dataset [36,37] available at https://wateriso.utah.edu/waterisotopes/index.html (accessed on 23 November 2026). These raster products in GeoTIFF format contain global maps of H and O isotope ratios for monthly and mean-annual amount-weighted precipitation at 5 arc-minute resolution. The corresponding $\delta^{18}O$ and $\delta^{2}H$ values were obtained for each cluster's latitude, longitude, and season. After that, the d-excess was calculated using the formula d-excess = $\delta^{2}H - 8 \times \delta^{18}O$ [5]. Resulting values from the calculation were appended and plotted using JMP®, Version 18.0.1. SAS Institute Inc., Cary, NC, USA, 1989–2023 (Supplementary Materials Figure S9—summer; Figure S10—winter).

Following the methodology for d-excess, tritium values were also spatially plotted in function of the trajectories of the obtained clusters (Supplementary Materials Figure S11—winter). The input gridded data for accomplishing this task was the MIROC5-iso with the specific CRAC_3H_cte.197901-201812.monmean.TU_precip.nc product with constant long-term average ^{3}H values over time, available at the Zenodo repository https://zenodo.org/records/10223858 (accessed on 23 November 2026) [38].

2.6. Multiple Linear Regression Analysis

To assess the additional explanatory contribution of convective precipitation fraction (CPF), multiple linear regression models were fitted separately for $\delta^{18}O$, $\delta^{2}H$, d-excess, and ^{3}H at each station. Baseline models included calendar-month seasonality, mean air temperature on precipitation days, and monthly precipitation amount. Extended models additionally incorporated CPF derived from SYNOP RK v11, ERA5, or GPM 3GCSH.

The additional explanatory contribution of CPF was quantified as $\Delta R^2 = R^2(\text{full model}) - R^2(\text{baseline model})$. Statistical inference for CPF coefficients was based on heteroskedasticity- and autocorrelation-consistent (HAC) standard errors estimated using the Newey–West method with a maximum lag of 12 months. HAC-based 95% confidence intervals and *p*-values were calculated for the CPF coefficients. The Benjamini–Hochberg procedure was applied to control the false discovery rate across multiple tests, with $q < 0.05$ considered statistically significant. Globally adjusted *p*-values were used for the primary interpretation. Models were estimated using available paired monthly observations for each

station, isotope variable, and precipitation product. Complete station-specific regression results, including sample sizes, CPF coefficients, 95% confidence intervals, Benjamini–Hochberg-adjusted *p*-values, and ΔR^2, are provided in Supplementary Table S4.

The Debrecen event-level analyses included 975 precipitation isotope records from two observation periods (2000–2009 and 2015–2018), of which 888 satisfied the isotope and ERA5 quality-control criteria. Isotope sampling days were matched with 6-hourly ERA5 precipitation and meteorological data, aggregated over the corresponding sampling intervals. Events were classified as stratiform (CPF ≤ 0.20), mixed ($0.20 < \text{CPF} < 0.80$), or convective (CPF ≥ 0.80). Stratiform–convective comparisons were restricted to observation-period and calendar-month strata containing both precipitation types, using equal-stratum and harmonic-sample-size weighting. Meteorological variables were precipitation-weighted, whereas regression models were fitted without additional event weighting. Temporal dependence was addressed using HAC standard errors with a maximum lag of seven successive observations, and multiple testing was controlled using the Benjamini–Hochberg procedure.

3. Results

3.1. SYNOPs, Quality Control and Statistics

Figure 2 presents the monthly climatological distribution of precipitation types at the six study stations, expressed as precipitation-amount-weighted fractions derived from the SYNOP RK v11 classification. The results reveal a pronounced seasonal cycle, with stratiform precipitation dominating during the colder months and convective precipitation increasing during the warm season. From November to February, stratiform precipitation generally accounts for more than 70% of the monthly precipitation amount. During summer, convective precipitation becomes dominant in Debrecen, Vienna, and Krakow, reaching approximately 75%, 60%, and 70%, respectively. In contrast, stratiform precipitation remains the dominant type throughout most of the year in Zagreb, Cuxhaven, and Wasserkuppe. Mixed precipitation exhibits a less pronounced seasonal cycle, with relatively high summer contributions in Debrecen, Zagreb, and Wasserkuppe. These seasonal differences reflect the combined influence of atmospheric instability, moisture availability, regional circulation, and local geographical conditions.

The corresponding monthly climatologies derived from ERA5 and GPM 3GCSH are presented in Supplementary Materials (Figure S2 and Figure S3, respectively). ERA5 indicates a stronger and more spatially consistent summer maximum in convective precipitation, whereas GPM generally shows a higher stratiform contribution and weaker seasonal variability. These differences highlight the sensitivity of precipitation-type estimates to the underlying data source and classification methodology.

The quantitative comparison of monthly convective precipitation fractions over the overlapping period (2014–2024) is summarized in Table 1. SYNOP RK v11 and ERA5 exhibit relatively strong correlations in Krakow ($r = 0.89$), Vienna ($r = 0.81$), Zagreb ($r = 0.75$), and Debrecen ($r = 0.65$), whereas agreement is weaker in Cuxhaven ($r = 0.44$) and Wasserkuppe ($r = 0.43$). Correlations involving GPM are generally lower ($r = 0.04$–0.40). ERA5 systematically estimates higher convective fractions than GPM, while SYNOP RK v11 yields substantially lower fractions than ERA5 in Cuxhaven, Wasserkuppe, and Zagreb.

The pronounced discrepancies at Cuxhaven and Wasserkuppe may partly reflect changes in SYNOP reporting practices, including the transition to automated observations. However, differences in classification methodology and temporal sampling must also be considered. Overall, the comparison demonstrates that the seasonal increase in convective precipitation is a common feature of the datasets, whereas its estimated magnitude remains method-dependent. Therefore, the agreement statistics in Table 1 are interpreted as measures of inter-dataset consistency rather than independent validation.

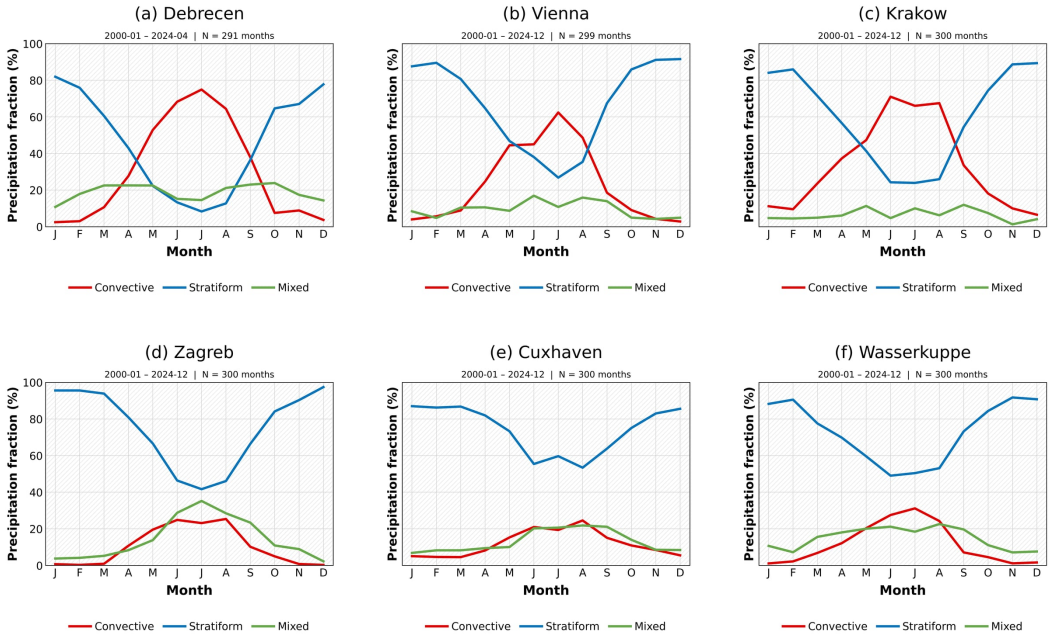

Figure 2. Monthly climatological precipitation amount fractions by precipitation type at the six study stations: (**a**) Debrecen (HU), (**b**) Vienna (AT), (**c**) Krakow (PL), (**d**) Zagreb (HR), (**e**) Cuxhaven (DE), and (**f**) Wasserkuppe (DE). Values represent the percentage contribution of convective, stratiform, and mixed precipitation to the total monthly precipitation amount, based on the precipitation-amount-weighted SYNOP classification (RK method) during the study period (2000–2024). Monthly climatological values were calculated by averaging the available monthly precipitation fractions for each calendar month. Unclassified precipitation was retained in the total precipitation amount but is not shown separately. The observation period and number of valid months (N) are indicated above each panel.

Table 1. Agreement between monthly convective precipitation fractions derived from SYNOP RK v11, ERA5, and GPM 3GCSH at six Central European stations during 2014–2024.

Station	N	SYNOP RK–GPM			ERA5–GPM			SYNOP RK–ERA5		
		Relative Bias (%)	NRMSE (%)	r	Relative Bias (%)	NRMSE (%)	r	Relative Bias (%)	NRMSE (%)	r
Cuxhaven †	127	−18.70	32.03	0.04	+17.42	28.09	0.21	−36.12	40.48	0.44
Debrecen	119	+22.15	42.48	0.28	+19.47	34.42	0.29	+2.69	27.02	0.65
Krakow	126	+22.59	38.83	0.38	+19.47	30.92	0.38	+3.13	16.69	0.89
Vienna	125	+12.76	32.51	0.40	+21.14	31.82	0.39	−8.38	20.47	0.81
Wasserkuppe †	127	−2.66	30.88	0.13	+23.51	33.83	0.29	−26.16	35.96	0.43
Zagreb	126	−7.61	32.08	0.31	+12.86	27.63	0.38	−20.47	28.51	0.75

Notes: N is the number of matched monthly observations. Bias is the first dataset minus the second dataset. Bias and normalized RMSE are expressed in percentage relative to the first value; r is Pearson's correlation coefficient. † Stations potentially affected by changes in SYNOP reporting practices, including automation.

3.2. Relationship Between Rainwater Isotopic Composition and Precipitation Types

The relationships between monthly precipitation-type fractions and precipitation $\delta^{18}O$, $\delta^{2}H$, d-excess, and ^{3}H were examined at six European stations using SYNOP RK v11, ERA5, and GPM 3GCSH data. Pearson correlations were first calculated from the original monthly series and subsequently from anomalies obtained by subtracting the corresponding calendar-month means. This approach allowed us to distinguish associations reflecting the combined seasonal and interannual variability from those persisting after removal of the mean seasonal cycle. Statistical significance of anomaly relationships was assessed using heteroskedasticity- and autocorrelation-consistent (HAC) standard errors and Benjamini–Hochberg false discovery rate (FDR) correction (Table 2).

Table 2. Pearson correlation coefficients (r) between monthly convective precipitation fractions and precipitation isotope composition ($\delta^{18}O$, $\delta^{2}H$, d-excess, and ^{3}H) at six European stations, based on SYNOP RK v11, ERA5, and GPM 3GCSH datasets. Correlations are reported for both the original monthly time series (raw) and calendar-month anomalies (anomaly), representing relationships before and after removal of the mean seasonal cycle, respectively. Statistical significance of anomaly correlations was assessed using heteroskedasticity- and autocorrelation-consistent (HAC) standard errors with a 12-month lag and Benjamini–Hochberg false discovery rate (FDR) correction. Asterisks (*) indicate significant anomaly correlations ($q < 0.05$). Sample sizes (N) represent the number of paired monthly observations. Missing values indicate insufficient overlapping data.

Station	Source	$\delta^{18}O$: Raw/Anomaly	$\delta^{2}H$: Raw/Anomaly	d-Excess: Raw/Anomaly	^{3}H: Raw/Anomaly
Cuxhaven	SYNOP RK v11	+0.34/+0.09 (N = 156)	+0.35/+0.10 (N = 156)	+0.01/+0.04 (N = 156)	+0.40/+0.21 (N = 264)
Cuxhaven	ERA5	+0.52/+0.20 (N = 156)	+0.54/+0.24 (N = 156)	+0.02/+0.14 * (N = 156)	+0.52/+0.12 (N = 264)
Cuxhaven	GPM 3GCSH	—	—	—	+0.12/−0.07 (N = 93)
Debrecen	SYNOP RK v11	+0.62/+0.18 (N = 190)	+0.64/+0.15 (N = 190)	−0.16/−0.12 (N = 190)	+0.62/+0.16 (N = 215)
Debrecen	ERA5	+0.74/+0.40 * (N = 191)	+0.77/+0.43 * (N = 191)	−0.16/−0.11 (N = 191)	+0.59/+0.11 (N = 216)
Debrecen	GPM 3GCSH	+0.35/+0.16 (N = 57)	+0.30/+0.09 (N = 57)	−0.31/−0.23 (N = 57)	+0.42/+0.27 (N = 57)
Krakow	SYNOP RK v11	+0.71/+0.36 * (N = 251)	+0.70/+0.34 * (N = 251)	−0.21/−0.14 * (N = 251)	+0.60/−0.04 (N = 250)
Krakow	ERA5	+0.80/+0.45 * (N = 251)	+0.79/+0.43 * (N = 251)	−0.22/−0.21 * (N = 251)	+0.70/+0.07 (N = 250)
Krakow	GPM 3GCSH	+0.34/+0.11 (N = 92)	+0.34/+0.12 (N = 92)	+0.02/+0.06 (N = 92)	+0.29/+0.08 (N = 92)
Vienna	SYNOP RK v11	+0.54/+0.13 (N = 266)	+0.54/+0.13 (N = 266)	−0.02/−0.05 (N = 266)	+0.58/+0.05 (N = 264)
Vienna	ERA5	+0.67/+0.31 * (N = 266)	+0.67/+0.31 * (N = 266)	−0.03/−0.05 (N = 266)	+0.68/+0.14 (N = 264)
Vienna	GPM 3GCSH	+0.24/−0.06 (N = 98)	+0.23/−0.05 (N = 98)	−0.07/+0.07 (N = 98)	+0.40/+0.15 (N = 101)
Wasserkuppe	SYNOP RK v11	+0.57/+0.26 * (N = 168)	+0.55/+0.28 * (N = 168)	−0.17/+0.15 (N = 168)	+0.42/+0.06 (N = 261)
Wasserkuppe	ERA5	+0.66/+0.31 * (N = 168)	+0.63/+0.32 * (N = 168)	−0.23/+0.14 (N = 168)	+0.56/+0.09 (N = 261)
Wasserkuppe	GPM 3GCSH	—	—	—	+0.22/+0.06 (N = 92)
Zagreb	SYNOP RK v11	+0.44/+0.11 (N = 166)	+0.43/+0.12 (N = 168)	−0.16/+0.05 (N = 166)	+0.41/+0.06 (N = 227)
Zagreb	ERA5	+0.76/+0.44 * (N = 166)	+0.75/+0.42 * (N = 168)	−0.30/−0.18 (N = 166)	+0.51/+0.03 (N = 227)
Zagreb	GPM 3GCSH	+0.16/+0.08 (N = 53)	+0.13/+0.08 (N = 53)	−0.24/−0.02 (N = 53)	+0.18/−0.03 (N = 56)

The original monthly series showed predominantly positive correlations between convective precipitation fractions and isotope composition. For $\delta^{18}O$, correlation coefficients ranged from 0.34 to 0.71 for SYNOP RK v11, 0.52 to 0.80 for ERA5, and 0.16 to 0.35 for GPM. Similar relationships were observed for $\delta^{2}H$. Positive correlations were also found for ^{3}H, with coefficients ranging from 0.40 to 0.62 for SYNOP RK v11, 0.51 to 0.70 for ERA5, and 0.12 to 0.42 for GPM. These associations indicate that months with higher convective precipitation fractions generally coincided with higher stable-isotope and tritium values. However, they may partly reflect the pronounced seasonal cycles shared by precipitation type and isotope composition.

After removal of the mean seasonal cycle, correlations weakened substantially, although significant relationships persisted for the stable isotopes. The most consistent results were obtained using ERA5 convective precipitation fractions. Anomaly correlations ranged from 0.20 to 0.45 for $\delta^{18}O$ and from 0.24 to 0.43 for $\delta^{2}H$, remaining positive and significant at five of the six stations after HAC–FDR correction ($q < 0.05$). The strongest relationships

occurred at Krakow ($\delta^{18}O$: r = 0.45; $\delta^{2}H$: r = 0.43), Zagreb (0.44; 0.42), and Debrecen (0.40; 0.43). At Cuxhaven, the correlations remained positive but were not statistically significant.

For SYNOP RK v11, significant positive anomaly correlations between convective precipitation and both stable isotopes were restricted to Krakow ($\delta^{18}O$: r = 0.35; $\delta^{2}H$: r = 0.34) and Wasserkuppe (0.26; 0.28). No significant relationships were identified for GPM after HAC–FDR correction. However, the shorter GPM record and the lack of overlapping stable-isotope observations at two stations limit direct comparisons among the three precipitation datasets. Differences in correlation strength therefore cannot be attributed solely to differences in precipitation-type classification.

In contrast, the positive associations between convective precipitation and ^{3}H largely disappeared after seasonal adjustment. Anomaly correlations ranged from −0.04 to 0.21 for SYNOP RK v11, 0.03 to 0.14 for ERA5, and −0.07 to 0.27 for GPM. None remained significant after HAC–FDR correction. This indicates that the positive relationships observed in the original monthly series were largely associated with shared seasonal variability rather than a consistent month-to-month relationship independent of the mean annual cycle. Nevertheless, these findings do not exclude possible influences of convective processes on precipitation tritium concentrations.

The relationships involving d-excess were less consistent. At Krakow, significant negative anomaly correlations with convective precipitation fractions were obtained using both ERA5 (r = −0.21) and SYNOP RK v11 (r = −0.14). Conversely, ERA5 indicated a weak positive relationship at Cuxhaven (r = 0.14). These contrasting signs suggest that no uniform regional relationship exists between d-excess and convective precipitation fractions. Additional significant correlations involving stratiform and mixed precipitation are reported in Supplementary Table S5. The opposite signs of ERA5 convective and stratiform correlations should not be interpreted as independent evidence because the two precipitation fractions are complementary.

Overall, the positive association between convective precipitation fractions and stable-isotope composition cannot be explained entirely by their shared mean seasonal cycle, particularly in the ERA5 dataset. In contrast, the absence of significant ^{3}H anomaly correlations suggests that the seasonal covariation between tritium and convective precipitation does not extend to a consistent relationship at the monthly anomaly scale. These differences indicate that stable-isotope and tritium variability may respond to distinct atmospheric controls. However, the remaining stable-isotope correlations do not establish a direct causal influence of convective precipitation, as temperature, precipitation amount, moisture provenance, and atmospheric circulation may also contribute to the observed relationships. Their relative roles are investigated in the following multivariate analyses.

3.3. Additional Explanatory Contribution of Convective Precipitation Beyond Seasonality

To determine whether convective precipitation fraction (CPF) provides additional explanatory information beyond the shared seasonal cycle and meteorological variability, we performed multiple linear regression analyses for $\delta^{18}O$, $\delta^{2}H$, d-excess, and ^{3}H at the six monitoring stations.

The baseline models included calendar-month seasonality, precipitation, day mean air temperature, and monthly precipitation amount. Extended models additionally incorporated monthly CPF derived from SYNOP RK v11, ERA5, or GPM 3GCSH. The additional explanatory contribution of CPF was quantified as the difference between the coefficients of determination of the extended and baseline models (ΔR^{2}). Statistical significance was assessed using HAC-robust standard errors and Benjamini–Hochberg correction.

For SYNOP RK v11, the additional explanatory contribution of CPF was generally small. The median ΔR^{2} across the six stations was 0.0030 for $\delta^{18}O$ and 0.0022 for $\delta^{2}H$, corresponding

to additional explained variance of 0.30 and 0.22 percentage points, respectively. Statistically significant positive associations were identified at Krakow, whereas the other stations did not show significant additional CPF contributions after multiple-testing correction.

ERA5-derived CPF provided a larger additional explanatory contribution to stable isotope variability. The median ΔR^2 was 0.0158 for $\delta^{18}O$ and 0.0171 for δ^2H, corresponding to 1.58 and 1.71 additional percentage points of explained variance, respectively. Significant associations were identified at Debrecen and Krakow. At Debrecen, CPF increased the explained variance by 2.25 percentage points for $\delta^{18}O$ and 1.72 percentage points for δ^2H. At Krakow, the corresponding increases were 2.04 and 2.01 percentage points.

For GPM 3GCSH, the additional explanatory contribution was generally limited. The median ΔR^2 was 0.0043 for $\delta^{18}O$, 0.0034 for δ^2H, and 0.0056 for d-excess. For ^3H, the median ΔR^2 was 0.0037. No statistically significant CPF contributions were identified after multiple-testing correction. However, the shorter GPM observation period and the limited overlap with stable-isotope records constrain direct comparisons with SYNOP and ERA5.

For d-excess and ^3H, no statistically significant additional contributions of CPF were detected after multiple-testing correction, regardless of the precipitation product. This contrasts with the stable isotope results and indicates that the explanatory contribution of precipitation regime differs among isotope variables.

Overall, the multivariable analyses demonstrate that convective precipitation fraction provides a modest but statistically detectable additional contribution to $\delta^{18}O$ and δ^2H variability at selected stations, particularly Debrecen and Krakow. Nevertheless, most of the explained variance was already captured by the seasonal and meteorological predictors. The magnitude and significance of the additional CPF contribution also depended on the precipitation product, highlighting the methodological sensitivity of precipitation-type–isotope relationships.

3.3.1. Seasonal Covariation Between Oxygen-18 and Tritium

Table 3 summarizes the seasonal mean $\delta^{18}O$ and ^3H values for the six investigated stations during their respective observation periods within 2000–2018. Both isotope variables exhibit pronounced seasonal variability. In general, lower $\delta^{18}O$ and ^3H values occur during winter, followed by increasing values during spring and maxima during summer, before decreasing again in autumn. This common seasonal pattern is reflected in the positive relationships between $\delta^{18}O$ and ^3H shown in the left column of Figure 3.

Table 3. Seasonal mean rainwater isotopic values $\delta^{18}O$ (‰) and ^3H (TU) from Debrecen rainwater monitoring and the IAEA/GNIP stations for the period 2000–2018.

Station	Winter		Spring		Summer		Autumn	
	$\delta^{18}O$	^3H	$\delta^{18}O$	^3H	$\delta^{18}O$	^3H	$\delta^{18}O$	^3H
Debrecen	−11.00	7.82	−6.66	11.92	−4.63	13.38	−7.90	8.48
Vienna	−12.03	7.37	−8.74	10.52	−6.25	12.34	−9.88	8.37
Krakow	−12.98	6.83	−8.66	10.89	−6.42	12.95	−9.63	8.00
Zagreb	−12.17	6.11	−7.25	8.86	−6.00	11.21	−8.53	6.73
Cuxhaven	−8.65	8.45	−6.86	11.17	−6.19	12.85	−7.26	10.46
Wasserkuppe	−10.94	7.30	−9.39	10.29	−7.22	10.87	−9.48	7.62

The strength of the climatological $\delta^{18}O$–^3H relationship varies among stations. Based on the long-term monthly means used in Figure 3, the coefficients of determination (R^2) are 0.78 for Debrecen, 0.88 for Vienna, and 0.86 for Krakow. Among the other stations, Cuxhaven also shows a strong climatological relationship ($R^2 = 0.84$), whereas weaker relationships are observed at Zagreb ($R^2 = 0.64$) and Wasserkuppe ($R^2 = 0.55$). Thus, despite differences

in the strength of the relationships among stations, $\delta^{18}O$ and ^{3}H exhibit broadly coherent seasonal variations across the investigated region. However, these relationships are based on only 12 climatological monthly means per station and therefore describe shared annual variability rather than independent associations at the monthly timescale.

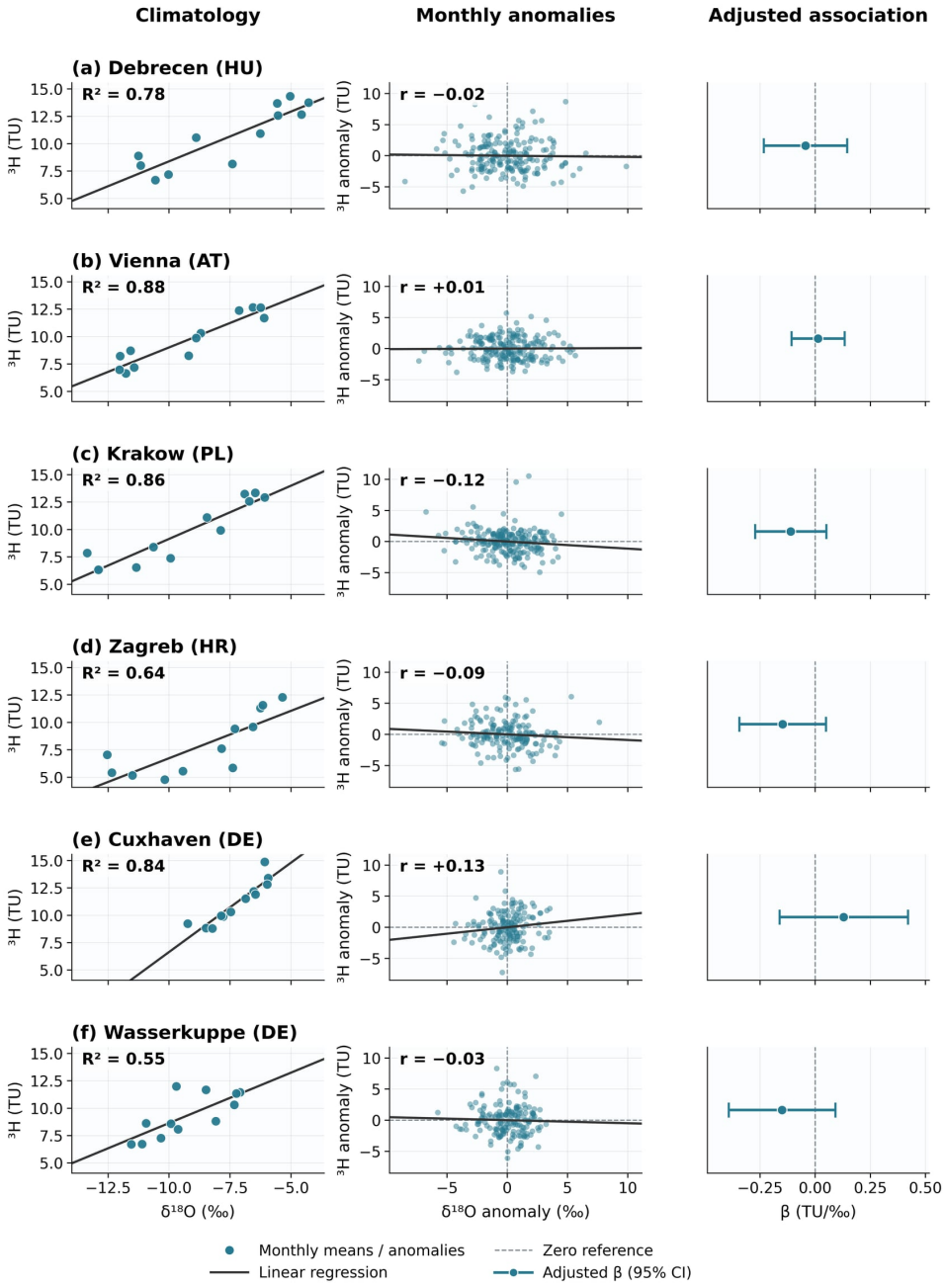

Figure 3. Seasonal and adjusted associations between precipitation $\delta^{18}O$ and tritium (^{3}H) activity at six European monitoring stations. **Left**: Relationships between the 12 long-term monthly climatological means, with linear regression lines and coefficients of determination (R^2). **Middle**: Relationships between monthly $\delta^{18}O$ and ^{3}H anomalies after removing calendar-month climatological means; r denotes the Pearson correlation coefficient. **Right**: Adjusted $\delta^{18}O$ regression coefficients (β, TU/‰) and 95% confidence intervals from multiple linear regression models controlling for calendar-month seasonality, precipitation-day mean temperature, and monthly precipitation amount. Confidence intervals were calculated using heteroskedasticity- and autocorrelation-consistent (HAC) standard errors with 12 lags. Dashed lines indicate zero association. Station-specific sample sizes and Benjamini–Hochberg-adjusted q-values are reported in Table 4.

Table 4. Relationships between monthly precipitation $\delta^{18}O$ and tritium (^3H) activity at six European monitoring stations after accounting for calendar-month seasonality, precipitation-day mean air temperature, and monthly precipitation amount. The analysis uses available paired monthly observations within 2000–2018.

Station	N	Anomaly r	Partial r	β (TU/‰)	95% HAC CI	ΔR^2	BH q
Debrecen	191	−0.019	−0.040	−0.044	[−0.233, 0.145]	0.0008	0.773
Vienna	212	+0.011	+0.015	+0.013	[−0.108, 0.133]	0.0001	0.835
Krakow	214	−0.121	−0.102	−0.111	[−0.273, 0.051]	0.0033	0.441
Zagreb	166	−0.087	−0.116	−0.148	[−0.344, 0.048]	0.0054	0.441
Cuxhaven	156	+0.128	+0.075	+0.129	[−0.162, 0.420]	0.0033	0.574
Wasserkuppe	166	−0.034	−0.092	−0.150	[−0.392, 0.091]	0.0051	0.441

Notes: N is the number of complete paired monthly observations. Anomaly r denotes the Pearson correlation after removing calendar-month climatological means, whereas partial r represents the association adjusted for calendar-month fixed effects, precipitation-day mean temperature, and monthly precipitation amount. β is the adjusted regression coefficient (TU/‰), and ΔR^2 is the additional proportion of total tritium variance explained by $\delta^{18}O$. The 95% confidence intervals were calculated using heteroskedasticity- and autocorrelation-consistent (HAC) standard errors with a maximum lag of 12 months. BH q-values represent Benjamini–Hochberg-adjusted *p*-values across the six station-specific tests.

To examine whether the $\delta^{18}O$–^3H relationship persists beyond the common seasonal cycle, the analysis was extended to individual paired monthly observations. Calendar-month seasonality was first removed by subtracting the corresponding long-term monthly means from each observation. The resulting anomaly correlations were substantially weaker than the climatological relationships (Figure 3, middle column), ranging from −0.121 at Krakow to +0.128 at Cuxhaven. Particularly weak correlations were observed at Debrecen ($r = -0.019$) and Vienna ($r = +0.011$), despite the strong positive relationships between their climatological monthly means.

The associations were further examined using station-specific multiple linear regression models with monthly ^3H activity as the response variable and $\delta^{18}O$ as the predictor of interest. Calendar-month fixed effects, precipitation-day mean air temperature, and monthly precipitation amount were included as covariates. The models were fitted to 156–214 paired monthly observations per station, depending on data availability. After adjustment for seasonal and meteorological variability, partial correlation coefficients ranged from −0.116 at Zagreb to +0.075 at Cuxhaven (Table 4). The corresponding $\delta^{18}O$ regression coefficients ranged from −0.150 to +0.129 TU/‰ (Figure 3, right column).

None of the adjusted associations were statistically significant. All 95% confidence intervals calculated using heteroskedasticity- and autocorrelation-consistent (HAC) standard errors included zero, and none of the six station-specific tests remained significant after Benjamini–Hochberg correction ($q \geq 0.441$). Moreover, the additional explanatory contribution of $\delta^{18}O$ was small, with incremental coefficients of determination (ΔR^2) ranging from 0.0001 to 0.0054. Thus, including $\delta^{18}O$ increased the explained monthly ^3H variance by no more than approximately 0.54 percentage points beyond the seasonal and meteorological covariates. Sensitivity analyses including a linear time trend yielded similar results, while forward-chaining cross-validation showed no consistent improvement in ^3H prediction when $\delta^{18}O$ was added to the baseline models.

Similar associations between precipitation $\delta^{18}O$ and ^3H and their relationship with precipitation type have previously been reported by previous study [14]. Therefore, the positive climatological $\delta^{18}O$–^3H relationships observed here are not interpreted as evidence for a previously unidentified direct coupling between the two isotope systems. Rather, the present six-station dataset demonstrates that their seasonal covariation is evident across the investigated Central European stations, while the monthly scale analysis indicates that this relationship becomes weak after accounting for the annual cycle and meteorological variability.

Importantly, the correlation between $\delta^{18}O$ and ^{3}H does not demonstrate that the two isotope variables are controlled by the same atmospheric process. In midlatitude precipitation, seasonal variations in $\delta^{18}O$ reflect changes in condensation conditions, temperature, moisture transport, and precipitation history. The seasonal cycle of precipitation ^{3}H additionally reflects variations in the tritium content and transport history of atmospheric moisture. Consequently, similar seasonal maxima of $\delta^{18}O$ and ^{3}H can produce strong climatological correlations even when the processes governing their variability are not identical. The absence of statistically significant adjusted associations further supports a cautious interpretation of the observed relationships as seasonal covariation rather than evidence of a direct or independently predictive coupling. The potential influence of atmospheric transport and moisture provenance is evaluated separately in the subsequent analyses.

3.3.2. Behavior of Deuterium Excess in Different Precipitation Types

Deuterium excess (d-excess) and Local Meteoric Water Lines (LMWLs) were examined to characterize regional differences in precipitation stable-isotope composition. To ensure methodological consistency, LMWLs were calculated using monthly $\delta^{18}O$ and $\delta^{2}H$ observations at all six stations (Figure 4). This approach eliminates differences in temporal resolution that could affect the regression parameters and their comparison among stations.

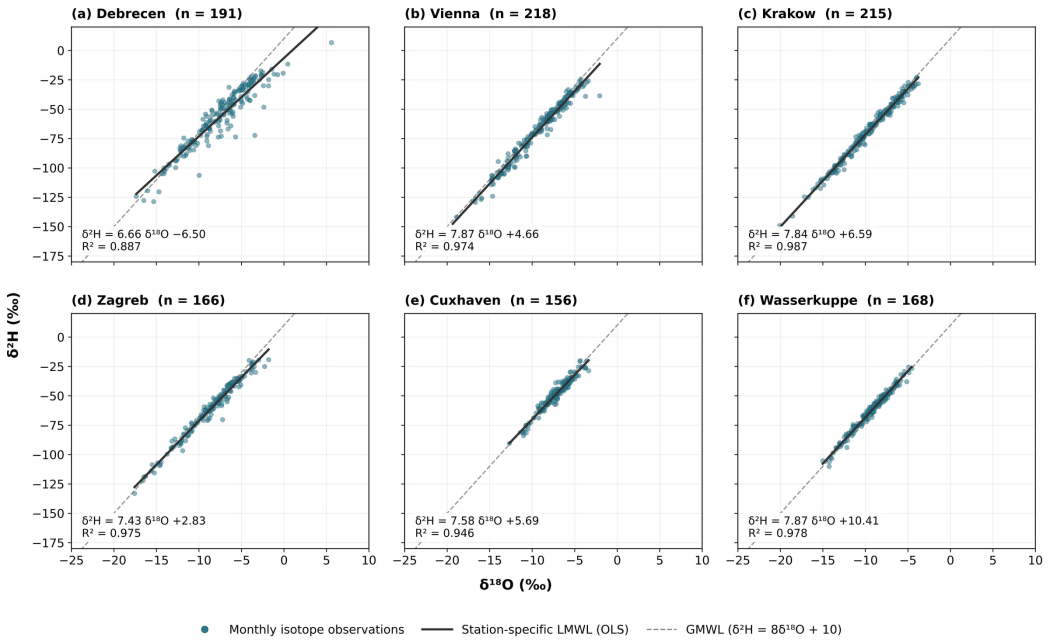

Figure 4. Local Meteoric Water Lines (LMWLs) derived from monthly precipitation $\delta^{18}O$ and $\delta^{2}H$ observations during the 2000–2018 study period at (**a**) Debrecen (HU), (**b**) Vienna (AT), (**c**) Krakow (PL), (**d**) Zagreb (HR), (**e**) Cuxhaven (DE), and (**f**) Wasserkuppe (DE). Each point represents a paired monthly isotope observation. Solid lines indicate station-specific ordinary least-squares regressions, while dashed lines represent the Global Meteoric Water Line (GMWL; $\delta^{2}H = 8\delta^{18}O + 10‰$). Regression equations, coefficients of determination (R^2), and sample sizes (n) are provided in each panel. All LMWLs were calculated at a consistent monthly temporal resolution.

The monthly LMWLs showed strong linear relationships between $\delta^{18}O$ and $\delta^{2}H$ at all stations, with coefficients of determination (R^2) ranging from 0.887 to 0.987. Debrecen exhibited the lowest slope (6.66) and a negative intercept (−6.50‰), together with the lowest mean d-excess (3.59‰). In contrast, the other five stations showed higher slopes (7.43–7.87) and positive intercepts (2.83–10.41‰). The highest mean d-excess was observed at Wasserkuppe (11.59‰), followed by Cuxhaven (8.74‰) and Krakow (8.14‰). These

results indicate that the monthly LMWL at Debrecen exhibits the largest deviation in slope from the Global Meteoric Water Line (GMWL) among the investigated stations.

Lower LMWL slopes and d-excess values may be associated with kinetic isotope fractionation, including below-cloud evaporation under unsaturated atmospheric conditions. However, these characteristics are not unique indicators of evaporation or convective precipitation processes. Differences in moisture provenance, atmospheric transport, condensation history, and local meteorological conditions may also influence the observed isotope relationships. Furthermore, although the temporal resolution was standardized, the available observation periods differed among stations, ranging from 2000 to 2012 at Cuxhaven to 2000–2018 at several other stations. Therefore, the observed spatial differences should not be attributed exclusively to precipitation type or any single atmospheric process.

The monthly LMWL results complement the precipitation-type correlation analysis presented in Section 3.2, where no consistent regional relationship was identified between convective precipitation fractions and d-excess anomalies. Together, these findings suggest that regional variations in precipitation isotope relationships reflect multiple interacting atmospheric influences rather than a uniform effect of convective precipitation.

To further examine precipitation-type-dependent isotope variability, an event-scale analysis was conducted for Debrecen using 876 quality-controlled precipitation samples. Mean d-excess values were 5.96‰, 4.93‰, and 3.22‰ for stratiform (n = 267), mixed (n = 348), and convective (n = 261) precipitation, respectively (Figure 5a–c). Comparisons matched by calendar month and observation period (n = 442) revealed significantly higher $\delta^{18}O$ (+2.12‰; 95% CI: +0.60 to +3.64‰) and $\delta^{2}H$ (+13.03‰; 95% CI: +2.14 to +23.92‰), but lower d-excess (−3.94‰; 95% CI: −6.67 to −1.21‰), in convective relative to stratiform precipitation. All three differences remained significant after Benjamini–Hochberg correction (adjusted $p \leq 0.019$).

The convective–stratiform d-excess difference decreased from −3.08‰ ($p = 0.0046$) to −1.87‰ ($p = 0.124$) after adjustment for relative humidity, temperature, and precipitation amount (Figure 5d,e). Event-scale precipitation-weighted relative humidity was positively associated with d-excess ($\beta = +0.092$‰ per percentage point; $p = 0.0048$; Figure 5f), whereas ERA5 surface evaporation showed no significant association ($p = 0.632$). Formal tests of local meteoric water line (LMWL) slope differences showed sensitivity to model specification. Although the month- and period-adjusted model indicated a nominally significant convective–stratiform slope difference ($p = 0.018$), this association did not remain significant after correction for multiple testing (BH-adjusted $p = 0.054$; Table S6). Furthermore, the difference between observation periods was not statistically significant ($p = 0.258$). These findings indicate that precipitation type is associated with isotopic variability beyond the seasonal cycle, although the available observations do not establish below-cloud evaporation as the underlying mechanism.

3.4. Clustered Trajectories

The bulk HYSPLIT backward trajectories calculated at 500, 1500, 3000 and 5000 m above sea level (ASL) are presented in Supplementary Figures S4–S7. In general terms, the trajectories indicate predominantly westerly air-mass transport toward the investigated stations. There is a consistent pattern of air parcel trajectories from west to east feeding the stations. In particular, it is noticeable that at lower levels (500 and 1500 m ASL) the Central European stations depict a branch of trajectories, especially during summertime, with an Atlantic origin. This path seems to merge into a more robust pattern from 3000 to 5000 m ASL. It is also noteworthy that the eastern and Mediterranean contributions during winter, spring, and autumn are also for the Central European stations. These sensitivity analyses at different altitudes suggest the presence of common regional air-mass transport

pathways. Therefore, the 3000 m ASL trajectories were selected to characterize the prevailing large-scale atmospheric transport patterns, without assuming that they directly represent near-surface conditions.

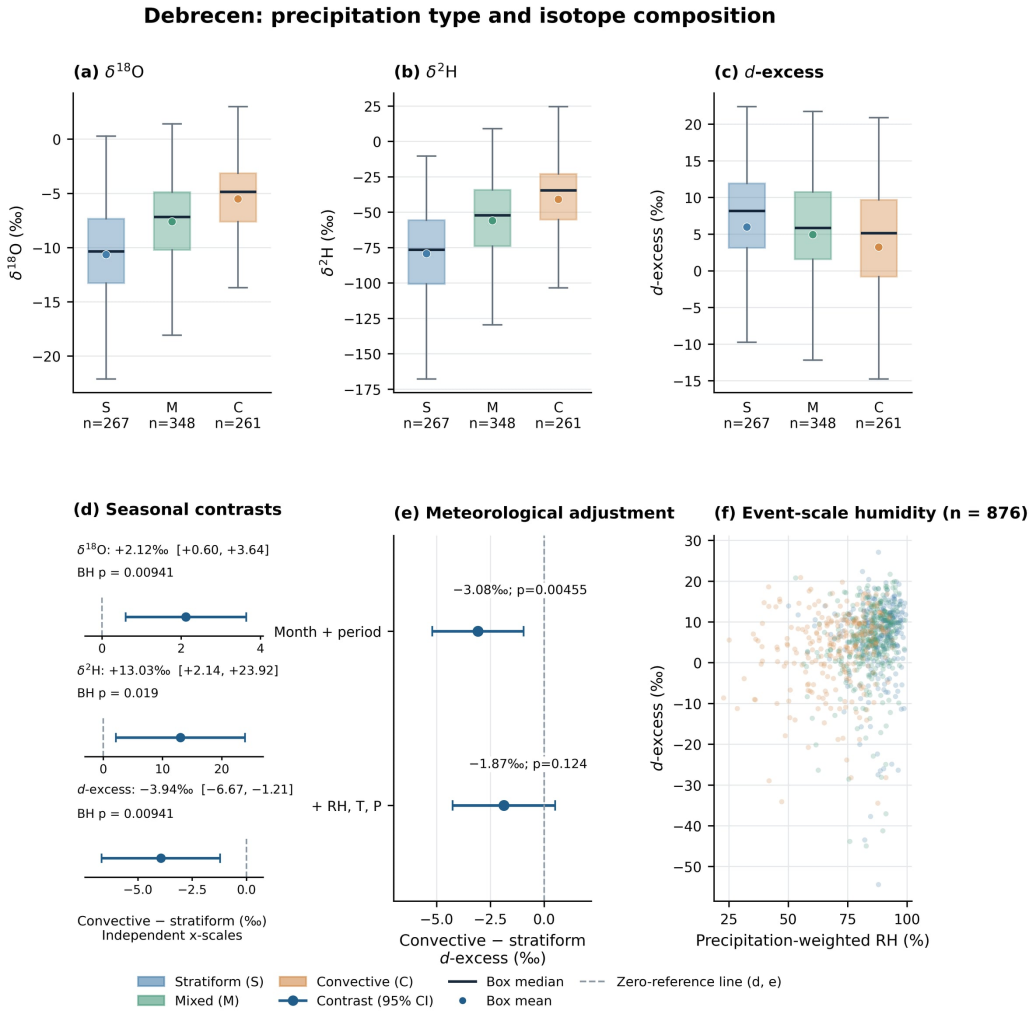

Figure 5. Precipitation-type-dependent isotope characteristics at Debrecen. (**a**–**c**) Event-scale distributions of $\delta^{18}O$, $\delta^{2}H$, and d-excess for stratiform, mixed, and convective precipitation (n = 876). Boxes indicate the interquartile range, horizontal lines represent medians, and whiskers extend to 1.5 times the interquartile range; dots indicate means. Outliers are omitted from the visualization but retained in the statistical analyses. (**d**) Seasonally matched convective–stratiform differences in $\delta^{18}O$, $\delta^{2}H$, and d-excess, based on 442 events from 20 calendar-month × observation-period strata. (**e**) Convective–stratiform d-excess differences before and after adjustment for relative humidity, temperature, and precipitation amount. Error bars indicate 95% confidence intervals based on heteroskedasticity- and autocorrelation-consistent (HAC) standard errors. (**f**) Relationship between event-scale precipitation-weighted relative humidity and d-excess, colored by precipitation type. The observed associations do not establish a unique causal mechanism.

3.4.1. General Clustered Trajectories

The main trajectories are summarized in Figure 6, which shows the five main clustered backward-trajectory pathways for each station during summer (JJA) over the 2005–2018 period. The corresponding clustered trajectories for the other seasons (DJF, MAM, and SON) are presented in Supplementary Figure S8.

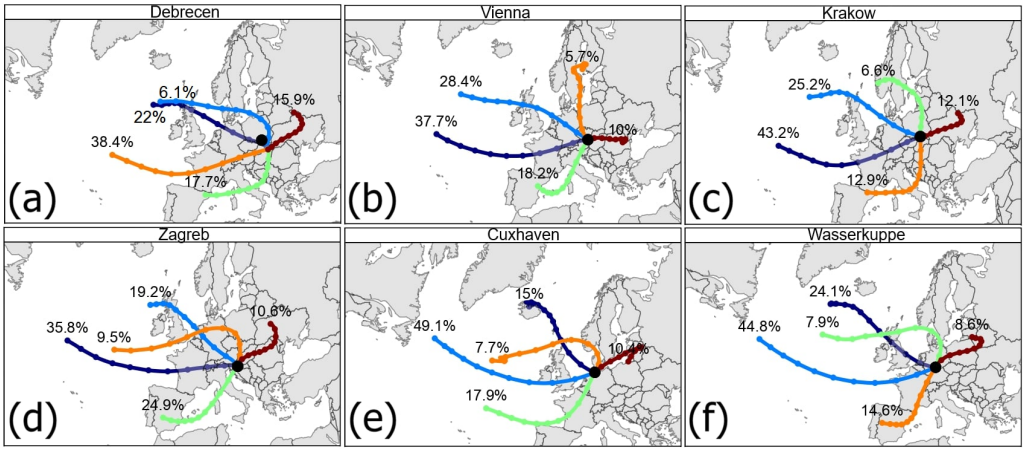

Figure 6. Summer cluster trajectories (2005–2018; 3000 m ASL) for (**a**) Debrecen (HU); (**b**) Vienna (AT); (**c**) Krakow (PL); (**d**) Zagreb (HR); (**e**) Cuxhaven (DE) and (**f**) Wasserkuppe (DE). The five trajectory clusters are distinguished by color: dark blue (Cluster 1), light blue (Cluster 2), green (Cluster 3), orange (Cluster 4), and dark red (Cluster 5). Colored lines represent the mean pathways of the corresponding trajectory clusters, while the small colored dots indicate successive positions along these pathways. Large black circles mark the receptor locations. Percentage labels indicate the relative frequency of each trajectory cluster during the study period. The same color scheme is applied consistently across all six stations to facilitate comparison of the dominant air-mass transport pathways.

The six stations exhibit several recurrent large-scale transport pathways, including trajectories crossing the North Atlantic, Scandinavia, the Mediterranean region, and continental eastern and western Europe. Atlantic pathways account for a substantial proportion of the trajectories reaching the investigated stations, although their relative frequency and geographical configuration vary among stations and seasons.

At Debrecen, the summer trajectory clusters are more regionally confined over continental Europe than during the other seasons, while Scandinavian pathways are less frequent in JJA (Supplementary Figure S8). During winter, an additional southeastern pathway extending toward the Aegean region is apparent. Atlantic pathways remain frequent and include trajectories passing both north and south of the British Isles. Trajectories extending across the Mediterranean region are also present throughout the year.

Vienna and Krakow exhibit broadly similar large-scale transport patterns. Scandinavian pathways occur throughout much of the year but are less frequent during summer (<7%). Atlantic trajectories form two recurrent branches passing north and south of the British Isles, while trajectories extending across the Mediterranean region account for less than 20% of the total trajectories.

At Zagreb, Scandinavian pathways are mainly observed during winter, when they account for approximately 7.2% of the trajectories. Trajectories extending across the Mediterranean region occur in all seasons and account for approximately 25% of the total, while the summer circulation also includes a substantial Atlantic component.

At Cuxhaven and Wasserkuppe, trajectories crossing Scandinavia are uncommon during summer but become more frequent during winter, spring, and autumn. Overall, the trajectory analysis demonstrates both common large-scale atmospheric transport pathways among the six stations and pronounced seasonal and geographical differences in their relative occurrence. These trajectory frequencies describe air-mass transport rather than quantitative moisture-source contributions; the locations of diagnosed moisture uptake are therefore evaluated separately in the following analyses.

3.4.2. Clustered Trajectories of Deuterium Excess and Tritium

Figure 7 presents a seasonal overview of the d-excess at all the studied stations. It is clear that spring (MAM) and summer (JJA) display the lowest d-excess values, whereas the autumn (SON) and winter (DJF) present higher values. This seasonal pattern is particularly pronounced at Wasserkuppe, where d-excess values remain above 10‰ during most of the year. The persistent westerly circulation at Wasserkuppe (Figure 1b,c) may contribute to this pattern; however, differences among stations may also reflect variations in moisture source, atmospheric transport, and local meteorological conditions.

Supplementary Materials Figures S9 and S10 place the clustered backward trajectories in the geographical context of gridded precipitation d-excess for summer and winter, respectively. Because the isotope-related values were assigned to the geographical coordinates crossed by the trajectories, these figures characterize the spatial isotope environment associated with the transport pathways rather than the isotope composition of individual air parcels. Figure S9 depicts the d-excess summer trajectories where different Atlantic, Mediterranean, northern European, and continental pathways encounter different ranges of d-excess values, and variability is also apparent along individual geographical pathways. Comparison with the winter results (Supplementary Figure S10) indicates a seasonal contrast, with higher gridded d-excess values occurring more frequently along several winter pathways and lower values being more characteristic of the regions intersected by the summer trajectories. These patterns suggest that air masses reaching the investigated stations pass through regions with different precipitation d-excess characteristics. However, they do not represent changes in the d-excess of the transported air parcels themselves and therefore cannot be used to reconstruct isotope evolution along the trajectories.

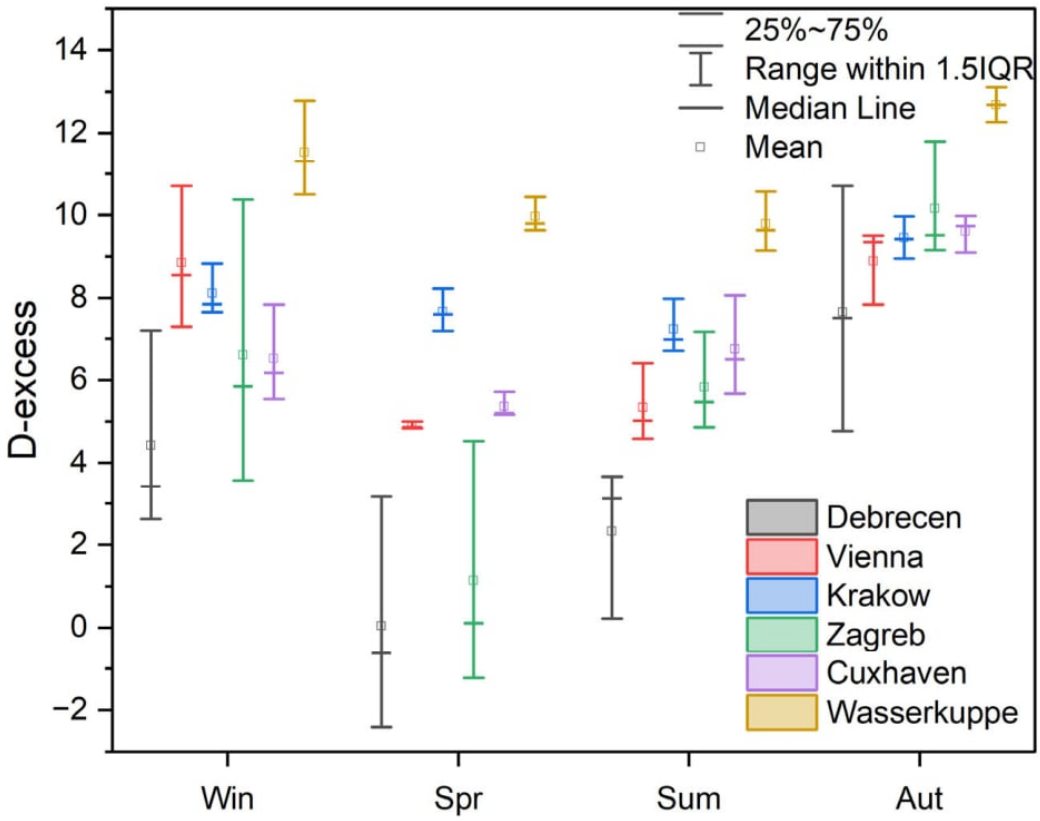

Figure 7. Seasonal d-excess boxplot for all the studied stations: Debrecen (HU), Vienna (AT), Krakow (PL), Zagreb (HR), Cuxhaven (DE) and Wasserkuppe (DE) for the period 2005–2018.

The tritium analysis provides a complementary geographical perspective as presented in Figure 8—summer (Supplementary Materials Figure S11—winter). In this case, the backward trajectories were compared with the spatial distribution of modeled precipitation ^{3}H concentration from the MIROC5-iso ^{3}H dataset. The trajectory pathways intersect regions characterized by different modeled ^{3}H values, demonstrating spatial heterogeneity in the tritium concentrations associated with the different transport pathways. However, the MIROC5-iso tritium values represent modeled precipitation tritium production rather than HTO concentration of individual air parcels. Consequently, the spatial patterns in Figure 7 cannot be interpreted as direct evidence that a particular trajectory transports tritium-rich moisture to the receptor station.

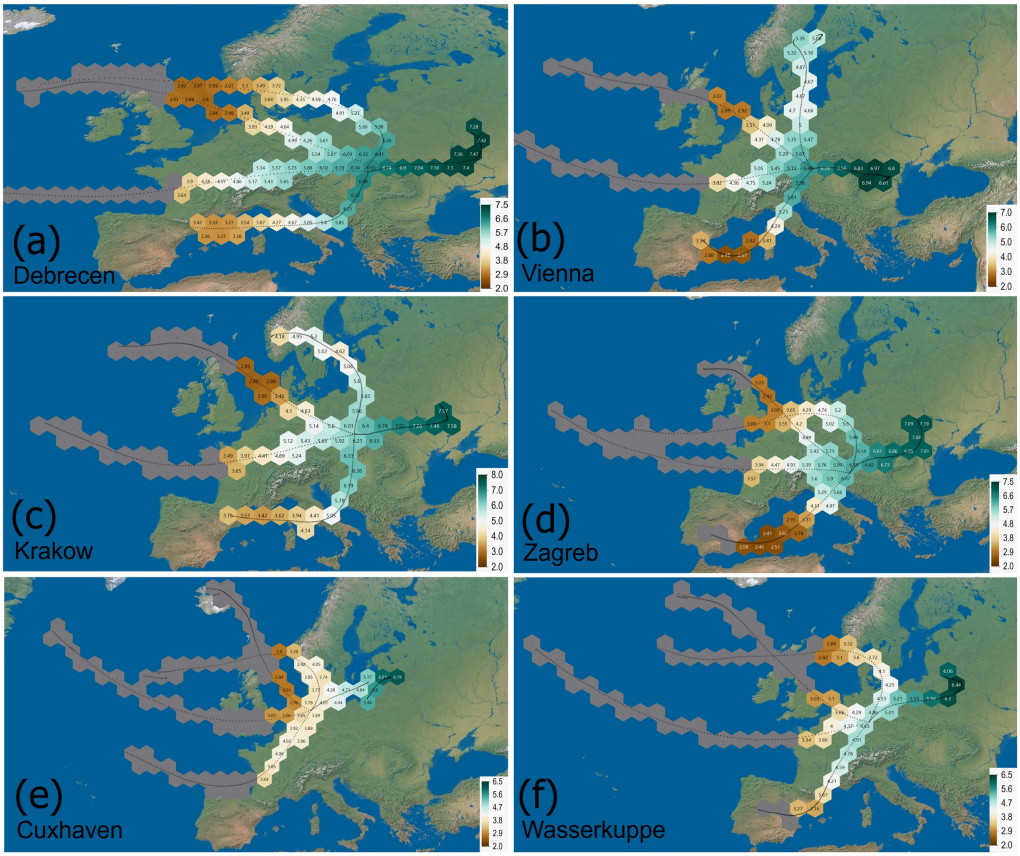

Figure 8. Summer cluster trajectories (2005–2018; 3000 m above sea level, ASL) with associated MIROC5-iso-simulated precipitation tritium concentrations (^{3}H, TU), based on long-term mean summer values, for (**a**) Debrecen (HU), (**b**) Vienna (AT), (**c**) Krakow (PL), (**d**) Zagreb (HR), (**e**) Cuxhaven (DE), and (**f**) Wasserkuppe (DE). Gray trajectories indicate locations where MIROC5-iso precipitation tritium data were unavailable.

Taken together (Figures 7 and S9–S11), they show that the air masses reaching the six stations follow geographically distinct pathways that intersect regions characterized by different precipitation d-excess and modeled atmospheric ^{3}H-production fields. These results provide a large-scale transport context for interpreting the isotope variability observed at the receptor stations. Nevertheless, the trajectory–isotope-field correspondence alone does not identify the geographical source of precipitating moisture, quantify source contributions, or establish a causal relationship between a particular transport pathway and the isotope composition measured in precipitation.

3.4.3. Seasonal Variability of Atmospheric Parameters and Precipitation Isotopes

Figure 9 summarizes the cloud parameters relevant to the $\delta^{18}O$, ^{3}H, and d-excess variability. A visual comparison of the same variables as a time series is presented in the Supplementary Materials, Figure S13.

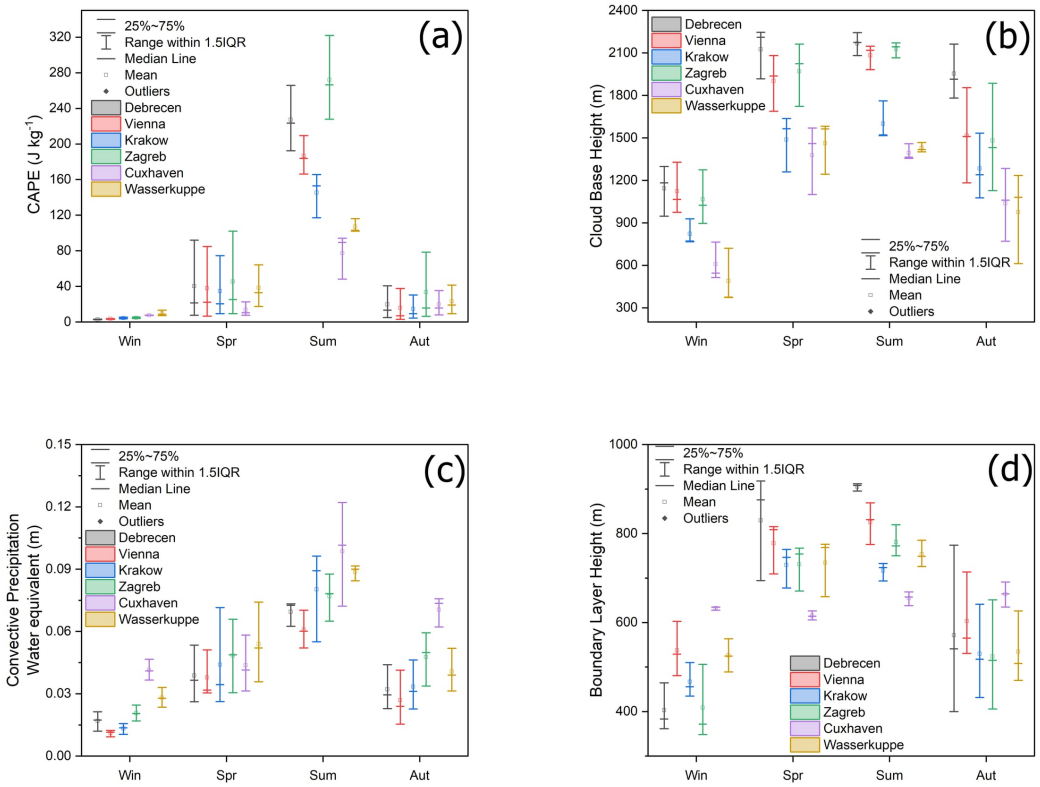

Figure 9. ERA5 boxplot of seasonal cloud parameters derived from ERA5 for (**a**) Convective Available Potential Energy CAPE, (**b**) Cloud Base Height (CBH), (**c**) Convective Precipitation, and (**d**) Boundary Layer Height (BLH).

The meteorological variables exhibit pronounced and consistent intra-annual patterns. CAPE, CBH, convective precipitation, and BLH generally increase from the colder to the warmer seasons, reaching their highest values in summer. Thereafter, CAPE and convective precipitation decrease more sharply, whereas CBH and BLH decline more gradually. This seasonal pattern is broadly consistent across the six stations.

Complementing the results, Figure 9 confirms that precipitation $\delta^{18}O$ and ^{3}H display pronounced temporal variability superimposed on a recurring seasonal cycle. Higher $\delta^{18}O$ and ^{3}H values generally occur during the warmer part of the year, broadly coinciding with the period of enhanced CAPE and greater boundary-layer development. However, individual isotope maxima do not consistently coincide with maxima in the meteorological variables. The correspondence is therefore interpreted primarily as a common seasonal pattern rather than as evidence that variations in CAPE, CBH, or BLH directly control precipitation $\delta^{18}O$ or ^{3}H. In contrast, d-excess exhibits a more irregular temporal pattern, including several pronounced short-term excursions, and does not show the same consistent seasonal correspondence with CAPE and BLH as $\delta^{18}O$ and ^{3}H. Similarly, no consistent temporal correspondence between d-excess and the moisture index is apparent from the monthly time series alone.

4. Discussion

4.1. SYNOPs

The present study was designed to investigate the relationship between precipitation type and the δ^2H, $\delta^{18}O$, and ^3H composition of precipitation at six Central European stations. Precipitation-type time series were derived from surface synoptic observations (SYNOP). The datasets cover approximately two decades, allowing convective, stratiform, and mixed precipitation events to be characterized over an extended period. Although observations at European synoptic stations are conducted under standardized conditions, occasional data gaps or observational uncertainties may still occur, which can affect the quality of the time series. Changes in the temporal resolution and completeness of SYNOPs may influence the reconstructed precipitation-type distributions and their temporal variability. These limitations are particularly noticeable in the case of mixed-type precipitation, where the classification of events may be less certain due to the limited temporal resolution and subjective interpretation of weather phenomena (e.g., Zagreb). Prior studies have noted the importance of contrasting the SYNOP dataset with other meteorological data for comparability of the same climatological characteristics [39]. Indeed, we tested the convective activity during summertime by using ERA5-convective cloud products CAPE, CBH, and BLH (Supplementary Materials Figure S13), giving consistent seasonality and summertime peaks. Despite these caveats, SYNOP-based datasets are generally considered reliable for climatological studies. Previous research [17] has demonstrated that precipitation types can be successfully separated based on station weather data and that such classifications are suitable for long-term climatological analyses. Therefore, SYNOP-derived time series provide a solid foundation for investigating the isotopic characteristics associated with different precipitation types.

Prior studies indicating the importance of convective and stratiform precipitation have shown that precipitation derived from convective clouds tends to have higher concentrations of both tritium and the heavy stable isotopes $\delta^{18}O$ and δ^2H [3,40]. Considering the elevations of the stations (Debrecen, 110 m; Vienna, 198 m; Krakow, 205 m; Zagreb, 157 m; Cuxhaven, 12 m; and Wasserkuppe, 921 m), the observed precipitation-type distributions are broadly consistent with previous studies reporting a greater occurrence of heavy convective precipitation at lower elevations and a greater contribution of heavy stratiform precipitation at higher elevations [17].

Debrecen, Vienna, and Krakow are characterized by a stronger continental climatic influence, whereas Zagreb and Cuxhaven are more strongly affected by maritime air masses. Wasserkuppe differs from the other stations primarily because of its substantially higher elevation (921 m), which influences its local meteorological conditions and precipitation regime (Figure 1). In stratiform precipitation, re-evaporation of falling hydrometeors in subsaturated layers can further modify the isotopic composition of precipitation [41]. Such post-condensation processes may contribute to the observed relationships between stratiform precipitation and stable isotope ratios, although the correlations cannot be attributed uniquely to this mechanism.

The higher occurrence of stratiform precipitation between November and February at the six stations (Figure 2) is consistent with the greater influence of extratropical cyclonic systems during the cold season. Midlatitude cyclones and their associated frontal systems commonly produce widespread stratiform precipitation, and their seasonal development is linked to the strength and position of the upper-level jet stream.

4.2. Tritium and Deuterium Excess in Convective Systems

Despite the importance of tritium and d-excess as hydrological tracers, there remains a paucity of evidence of their behavior in cloud processes at a seasonal scale, especially

in summertime. The clustered backward trajectories (Figures 7 and S9–S11) illustrate the seasonal variability of atmospheric transport pathways associated with precipitation isotope observations. The trajectories indicate that air masses reaching the investigated stations frequently passed over the Atlantic Ocean, the Mediterranean region, and continental Europe. However, these pathways represent potential transport corridors rather than quantitatively identified moisture sources. Because moisture uptake, loss, and isotopic evolution along individual trajectories were not calculated, the relative contributions of Atlantic, Mediterranean, and continental evaporation cannot be determined from the present analysis.

Seasonal changes in the spatial distribution of trajectories may reflect variations in large-scale atmospheric circulation, including the influence of the North Atlantic Oscillation and associated westerly flow [42,43]. Nevertheless, the present trajectory analysis does not establish a direct relationship between these circulation patterns and the observed d-excess variations. The spatial heterogeneity apparent in the hexagonally binned trajectory distributions (Supplementary Materials Figures S9–S11) indicates that the isotope observations are associated with a range of atmospheric transport pathways. However, discontinuities or localized variations in these distributions cannot be interpreted as direct evidence of local moisture uptake or recycling.

The d-excess time series exhibit substantial temporal variability and differences among stations (Supplementary Materials Figure S10). The isotopic composition of precipitation reflects the combined influence of moisture-source conditions, atmospheric transport, condensation, and post-condensation processes. Our event-scale analysis at Debrecen further demonstrated differences in d-excess between convective and stratiform precipitation after matching observations by calendar month and observation period. However, the precipitation-type contrast was not statistically significant after adjustment for the available meteorological covariates, and the analysis did not identify a unique evaporative mechanism. These findings emphasize the importance of high-resolution precipitation sampling for investigating processes that cannot be resolved using monthly isotope observations.

Although subcloud evaporation may modify precipitation isotope composition, the present results do not demonstrate that convective precipitation systematically experiences stronger evaporative modification than stratiform precipitation. Similarly, the possible effects of supersaturation during cold-season snowfall remain physically plausible but were not directly quantified in this study.

For tritium, the trajectory distributions and spatial patterns of the gridded precipitation-tritium product provide contextual information on broad atmospheric transport and regional variability, rather than direct evidence of specific moisture sources or recycling pathways. Previous studies have discussed the influence of continental and maritime air masses on precipitation tritium concentrations [41,44]. However, the present analysis cannot quantify the relative contributions of continental moisture, oceanic moisture, or individual atmospheric transport processes to the observed ^{3}H variability. Furthermore, the gridded tritium product represents model-simulated precipitation concentrations and should not be interpreted as a direct measurement of atmospheric tritium production or transport.

The positive correlations between convective precipitation fraction and ^{3}H observed in the original monthly series largely disappeared after removing the mean seasonal cycle. Furthermore, the multiple regression models did not identify statistically significant additional explanatory contributions of convective precipitation fraction to ^{3}H after accounting for seasonality, precipitation-day temperature, and precipitation amount. Consequently, the higher summertime tritium concentrations cannot be attributed specifically to convective moisture recycling or enhanced vertical transport on the basis of the present results.

For stable isotopes, the regression analyses revealed a different pattern. After accounting for calendar-month seasonality, precipitation-day temperature, precipitation amount, and temporal dependence, the additional explanatory contribution of convective precipitation fraction was generally modest and varied among stations. These findings indicate that precipitation-type information may provide complementary insights into stable-isotope variability at individual locations, but its explanatory value is not consistent across the investigated stations. Therefore, the combined use of precipitation-type indicators and isotope observations should be considered a complementary analytical approach rather than a universally robust diagnostic framework for identifying precipitation processes.

Tritium undergoes substantially less isotopic fractionation during phase changes than $\delta^{18}O$ and $\delta^{2}H$, and its atmospheric variability may be influenced by transport, mixing, and the distribution of tritium-bearing water reservoirs [45]. Nevertheless, precipitation ^{3}H concentrations alone do not provide a quantitative measure of vertical transport intensity or moisture-recycling timescales. The relationships between tritium and stable isotopes should therefore be interpreted in the context of their shared seasonal and atmospheric controls rather than as direct evidence of common cloud microphysical processes [46,47].

Between the 1960s and 1970s, there was an active interest in the study of clouds, in particular large convective hail clouds and the isotopic composition of hailstones [46,48]. Since then, researchers have recognized the importance of the physical processes within clouds, as their individual elements, such as droplets, drops, ice crystals and hailstones, provide valuable information about the prevailing thermodynamic conditions [49,50]. Similarly, the isotopic composition of $\delta^{2}H$, $\delta^{18}O$ and ^{3}H in hydrometeors has been used to examine the variability of $\delta^{2}H$ in droplets, raindrops, ice and graupels as a function of cloud temperature [49]. Moreover, they assisted in determining the kinetic effects occurring below the cloud base in subsaturated environments that affect raindrops [51]. In addition, hailstone growth histories were studied by their $\delta^{2}H$, ^{3}H isotopic layering [45,52,53]. A number of recent studies have corroborated the role that stratiform and convective types of precipitation have on the final isotopic values, especially at low latitudes [54–56]. Within convective systems, substantial isotopic variability arises depending on whether precipitation forms from local, regional, or large-scale moisture sources. In the case of locally driven convection—where the entrained vapor is predominantly recycled from near-surface evaporation—precipitation tends to exhibit isotopic enrichment, especially when clouds are shallow and the residence time for isotopic fractionation is short. In contrast, regional or large-scale moisture transport—such as oceanic vapor or long-range advection—undergoes progressive isotopic depletion due to Rayleigh-type distillation during transport. This typically results in depleted isotopic signatures in the resulting precipitation. The vertical structure and microphysical phase composition of hydrometeors also modulate isotopic signals. Systems dominated by ice-phase particles and associated with deep convection or long-range moisture transport generally promote isotopic depletion. Conversely, rapidly developing local systems with low cloud tops and a dominance of warm-liquid hydrometeors tend to preserve isotopically enriched characteristics of the source vapor.

In addition, according to the Copernicus latest report, 2024 was the warmest year on record for Europe, with an average temperature of 10.69 °C, which is 0.28 °C higher than the previous warmest year of 2020 and 2.92 °C above the 1850–1900 reference period [20,57]. As a result of this temperature rise, alterations in the precipitation processes have become more frequent and intense. It is expected, therefore, that more intense convective processes occur during the summer season, reducing the temperature control on the rainwater isotopic variability. The inclusion of cloud dynamics, precipitation formation at different vertical levels, and isotopic characterization of hydrometeors is necessary and pivotal for the future understanding of the hydrological cycle and the refinement of climate models [58].

Furthermore, the isotopic composition of precipitation, particularly variations in $\delta^{18}O$, $\delta^{2}H$, d-excess, and ^{3}H associated with different precipitation types, has direct implications for surface and groundwater recharge processes. Given that the isotopic signatures of recharge waters inherit the characteristics of meteoric input, understanding the seasonal and microphysical controls on rainwater isotopes is essential for improving hydrological models. Our findings highlight that convective precipitation, prevalent during summer, introduces isotopic signals that can substantially influence the temporal variability of aquifer recharge, streamflow isotopic composition, and tracer-based water balance studies in Central Europe. This connection emphasizes the critical need to incorporate precipitation type effects into hydrological modeling frameworks, especially under changing climate conditions that are projected to alter convective activity patterns.

5. Conclusions

This study investigated the relationships between precipitation type and the isotopic composition of precipitation ($\delta^{18}O$, $\delta^{2}H$, d-excess, and ^{3}H) at six European monitoring stations using SYNOP RK v11, ERA5, and GPM 3GCSH datasets. The results revealed pronounced seasonal covariability between convective precipitation fractions and precipitation isotope composition, particularly for $\delta^{18}O$ and $\delta^{2}H$.

After removing the mean seasonal cycle, positive associations between convective precipitation fractions and stable isotopes persisted at several stations, particularly in the ERA5 dataset. In contrast, the relationships involving ^{3}H weakened substantially, suggesting that their apparent association with convective precipitation largely reflected shared seasonality.

Multiple regression models accounting for seasonality, precipitation-day temperature, and precipitation amount demonstrated that convective precipitation fraction provides modest additional explanatory information for $\delta^{18}O$ and $\delta^{2}H$ at selected stations. The largest contributions were obtained using ERA5, with median increases in explained variance of 1.58 and 1.71 percentage points for $\delta^{18}O$ and $\delta^{2}H$, respectively. Significant additional contributions were identified mainly at Debrecen and Krakow, whereas SYNOP RK v11 showed smaller, station-dependent effects and GPM 3GCSH yielded no significant additional contributions.

For d-excess and ^{3}H, the additional contribution of the convective precipitation fraction was not statistically significant after multiple-testing correction. Event-scale analyses at Debrecen nevertheless revealed differences in stable isotope composition and d-excess between precipitation types, although these differences could not be attributed uniquely to subcloud evaporation.

Overall, the findings indicate that precipitation type provides limited but detectable additional information on stable isotope variability beyond seasonal and meteorological controls. However, the strength of these relationships depends on the station, isotope variable, and precipitation product, and the observed statistical associations should not be interpreted as direct evidence of causal atmospheric processes.

Supplementary Materials: The following supporting information can be downloaded at https://www.mdpi.com/article/10.3390/w18232975/s1 [38,59,60]. Figure S1: SYNOP-based precipitation regime classification and precipitation-amount-weighted monthly aggregation. Figure S2: Monthly climatological precipitation amount fractions derived from ERA5 at the six study stations; Figure S3: Monthly climatological convective and stratiform precipitation fractions derived from GPM 3GCSH at the six study stations; Figures S4–S7: HYSPLIT bulk back-trajectories 120 h (5 days) for the period 2005–2019; Figure S8: Back-trajectory paths grouped into five main clusters for the six European stations; Figure S9: Summer cluster trajectories and mean d-excess derived from the precipitation isoscape model; Figure S10: Winter cluster trajectories (2005–2018; 3000 m ASL) and their mean d-excess values calculated from monthly $\delta^{2}H$ and $\delta^{18}O$ values obtained from the precipi-

tation isoscape model. Figure S11: Winter cluster trajectories and tritium values derived from the MIROC5-iso:^{3}H model; Figure S12: Time-series comparison of precipitation ^{3}H values (TU; black line) and the proportions of SYNOP-classified convective (red line) and stratiform (blue line) precipitation from 2000 to 2018; Figure S13: ERA5- and CHELSA-derived cloud parameters compared with precipitation δ^{18}O, ^{3}H, and d-excess at the six study stations; Table S1: Temporal sensitivity of agreement between monthly convective precipitation fractions derived from SYNOP RK(C+M), ERA5, and GPM; Table S2: Summary of reported analytical uncertainties in precipitation tritium measurements at the six monitoring stations; Table S3: Temporal coverage and availability of monthly precipitation isotope observations at the six monitoring stations; Table S4: Station-specific regression results for the associations between convective precipitation fraction (CPF) and precipitation isotope composition (δ^{18}O, δ^{2}H, ^{3}H and d-excess), using the primary (core) model and full available observation periods; Table S5: Statistically significant correlations between monthly stratiform and mixed precipitation fractions and precipitation isotope composition at six European stations; Table S6: Sensitivity of precipitation-type differences in LMWL slopes at Debrecen.

Author Contributions: Conceptualization, E.L. and D.V.; methodology, E.L. and D.V.; software, E.L., D.V., Á.V. and Á.L.; validation, E.L., L.P. and M.B.; formal analysis, E.L., M.S.S. and M.B.; investigation, L.P.; resources, E.L. and L.P.; data curation, E.L. and L.P.; writing—original draft preparation, E.L. and D.V.; writing—review and editing, E.L., L.P. and D.V.; visualization, E.L. and D.V.; supervision, E.L.; project administration, E.L.; funding acquisition, E.L. and L.P. All authors have read and agreed to the published version of the manuscript.

Funding: The research leading to this paper was primarily supported by project 2020-2.1.1-ED-2021-00172, funded by the National Research, Development and Innovation Fund. Additional financial support was provided by the János Bolyai Research Scholarship of the Hungarian Academy of Sciences and the ÚNKP-23-5 New National Excellence Program of the Ministry for Innovation and Technology, financed from the National Research, Development and Innovation Fund.

Data Availability Statement: The data used in this study were obtained from publicly available databases and previously published sources, as described in the Materials and Methods section. These include meteorological and reanalysis data from SYNOP and ERA5, climatic data from CHELSA, precipitation isotope data from the IAEA Global Network of Isotopes in Precipitation (GNIP) and published sources, and gridded isotope and tritium products. Additional data supporting the findings of this study are available from the corresponding author upon reasonable request.

Acknowledgments: The authors gratefully acknowledge the institutions, organizations, and data providers that made the meteorological and isotope datasets used in this study available.

Conflicts of Interest: The authors declare no conflicts of interest. The funders had no role in the design of the study; in the collection, analyses, or interpretation of data; in the writing of the manuscript; or in the decision to publish the results.

Abbreviations

The following abbreviations are used in this manuscript:

ASL	Above Sea Level
AR(1)	First-Order Autoregressive Model
BLH	Boundary Layer Height
CAPE	Convective Available Potential Energy
CBH	Cloud Base Height
CHELSA	Climatologies at High Resolution for the Earth's Land Surface Areas
CRAC:^{3}H	Cosmic Ray Atmospheric Cascade: Tritium
d-excess	Deuterium Excess
DJF	December–January–February
ECMWF	European Centre for Medium-Range Weather Forecasts
ERA5	Fifth-Generation ECMWF Atmospheric Reanalysis
GDAS	Global Data Assimilation System
GMWL	Global Meteoric Water Line

GNIP	Global Network of Isotopes in Precipitation
GPM	Global Precipitation Measurement
3GCSH	Gridded Convective–Stratiform Heating
HTO	Tritiated Water
HYSPLIT	Hybrid Single-Particle Lagrangian Integrated Trajectory
IAEA	International Atomic Energy Agency
IRMS	Isotope Ratio Mass Spectrometry
JJA	June–July–August
LGR	Los Gatos Research
LMWL	Local Meteoric Water Line
LWIA	Liquid Water Isotope Analyzer
MAM	March–April–May
NAO	North Atlantic Oscillation
PSD	Power Spectral Density
SLAP	Standard Light Antarctic Precipitation
SON	September–October–November
SYNOP	Surface Synoptic Observations
TU	Tritium Unit
VSMOW	Vienna Standard Mean Ocean Water
WMO	World Meteorological Organization

References

1. Araguas, L.A.; Danesi, P.; Froehlich, K.; Rozanski, K. Global Monitoring of the Isotopic Composition of Precipitation. *J. Radioanal. Nucl. Chem. Artic.* **1996**, *205*, 189–200. [CrossRef]
2. Clark, I. *Groundwater Geochemistry and Isotopes*; CRC Press: New York, NY, USA, 2015; ISBN 978-1-4665-9173-8.
3. Dansgaard, W. Stable Isotopes in Precipitation. *Tellus* **1964**, *16*, 436–468. [CrossRef]
4. Rozanski, K.; Araguás-Araguás, L.J.; Gonfiantini, R. Isotopic Patterns in Modern Global Precipitation. *Clim. Change Cont. Isot. Rec.* **1993**, *78*, 1–36.
5. Clark, I.D.; Fritz, P. *Environmental Isotopes in Hydrogeology*; CRC Press: Boca Raton, FL, USA, 1997.
6. Froehlich, K.; Gibson, J.J.; Aggarwal, P. Deuterium Excess in Precipitation and Its Climatological Significance. In *International Conference on the Study of Environmental Change Using Isotope Techniques, Vienna, Austria, 23 April–27 December 2001*; International Atomic Energy Agency (IAEA): Vienna, Austria, 2002; Volume 13 (IAEA-CSP-13/P), pp. 54–66. Available online: https://inis.iaea.org/records/50trx-hjw91 (accessed on 23 November 2026).
7. Natali, S.; Doveri, M.; Giannecchini, R.; Baneschi, I.; Zanchetta, G. Is the Deuterium Excess in Precipitation a Reliable Tracer of Moisture Sources and Water Resources Fate in the Western Mediterranean? New Insights from Apuan Alps (Italy). *J. Hydrol.* **2022**, *614*, 128497. [CrossRef]
8. Cauquoin, A.; Fourré, É.; Landais, A.; Okazaki, A.; Yoshimura, K. Modeling Natural Tritium in Precipitation and Its Dependence on Decadal Solar Activity Variations Using the Atmospheric General Circulation Model MIROC5-Iso. *J. Geophys. Res. Atmos.* **2024**, *129*, e2023JD039745. [CrossRef]
9. Gat, J.R. Oxygen and Hydrogen Isotopes in the Hydrologic Cycle. *Annu. Rev. Earth Planet. Sci.* **1996**, *24*, 225–262. [CrossRef]
10. László, E.; Palcsu, L.; Leelőssy, Á. Estimation of the Solar-Induced Natural Variability of the Tritium Concentration of Precipitation in the Northern and Southern Hemisphere. *Atmos. Environ.* **2020**, *233*, 117605. [CrossRef]
11. Palcsu, L.; Morgenstern, U.; Sültenfuss, J.; Koltai, G.; László, E.; Temovski, M.; Major, Z.; Nagy, J.T.; Papp, L.; Varlam, C.; et al. Modulation of Cosmogenic Tritium in Meteoric Precipitation by the 11-Year Cycle of Solar Magnetic Field Activity. *Sci. Rep.* **2018**, *8*, 12813. [CrossRef]
12. Palcsu, L.; László, E.; Surányi, G.; Túri, M.; Vargas, D.; Veres, M.; Cauquoin, A.; Zákány, L.; Janovics, R.; Csige, I.; et al. Solar Cycle Detected in Natural Tritium of Ice Layers Before the Nuclear Era. *J. Geophys. Res. Atmos.* **2025**, *130*. [CrossRef]
13. Houze, R.A. *Cloud Dynamics*, 2nd ed.; International Geophysics: Amsterdam, The Netherlands, 2014.
14. Aggarwal, P.K.; Romatschke, U.; Araguas-Araguas, L.; Belachew, D.; Longstaffe, F.J.; Berg, P.; Schumacher, C.; Funk, A. Proportions of Convective and Stratiform Precipitation Revealed in Water Isotope Ratios. *Nat. Geosci.* **2016**, *9*, 624–629. [CrossRef]
15. Froehlich, K.; Kralik, M.; Papesch, W.; Rank, D.; Scheifinger, H.; Stichler, W. Deuterium Excess in Precipitation of Alpine Regions—Moisture Recycling. *Isot. Environ. Health Stud.* **2008**, *44*, 61–70. [CrossRef]
16. Beck, H.E.; Zimmermann, N.E.; McVicar, T.R.; Vergopolan, N.; Berg, A.; Wood, E.F. Present and Future Köppen-Geiger Climate Classification Maps at 1-Km Resolution. *Sci. Data* **2018**, *5*, 180214. [CrossRef]
17. Rulfová, Z.; Kyselý, J. Disaggregating Convective and Stratiform Precipitation from Station Weather Data. *Atmos. Res.* **2013**, *134*, 100–115. [CrossRef]

18. Tao, W.-K.; Lang, S.; Iguchi, T.; Song, Y. Goddard Latent Heating Retrieval Algorithm for TRMM and GPM. *J. Meteorol. Soc. Jpn.* **2022**, *100*, 293–320. [CrossRef]
19. Precipitation Processing System (PPS) at Goddard Space Flight Center. *GPM DPR (Gridded Convective Stratiform Heating) L3 1.5 Hours 0.5 Degree × 0.5 Degree V07*; NASA Goddard Space Flight Center: Greenbelt, MD, USA, 2022. Available online: https://www.earthdata.nasa.gov/data/catalog/ges-disc-gpm-3gcsh-07 (accessed on 23 November 2026).
20. Hersbach, H.; Bell, B.; Berrisford, P.; Hirahara, S.; Horányi, A.; Muñoz-Sabater, J.; Nicolas, J.; Peubey, C.; Radu, R.; Schepers, D.; et al. The ERA5 Global Reanalysis. *Q. J. R. Meteorol. Soc.* **2020**, *146*, 1999–2049. [CrossRef]
21. Karger, D.N.; Lange, S.; Hari, C.; Reyer, C.P.O.; Conrad, O.; Zimmermann, N.E.; Frieler, K. CHELSA-W5E5: Daily 1 Km Meteorological Forcing Data for Climate Impact Studies. *Earth Syst. Sci. Data* **2023**, *15*, 2445–2464. [CrossRef]
22. Schmidt, A.; Frank, G.; Stichler, W.; Duester, L.; Steinkopff, T.; Stumpp, C. Overview of Tritium Records from Precipitation and Surface Waters in Germany. *Hydrol. Process.* **2020**, *34*, 1489–1493. [CrossRef]
23. Stumpp, C.; Klaus, J.; Stichler, W. Analysis of Long-Term Stable Isotopic Composition in German Precipitation. *J. Hydrol.* **2014**, *517*, 351–361. [CrossRef]
24. Vodila, G.; Palcsu, L.; Futó, I.; Szántó, Z. A 9-Year Record of Stable Isotope Ratios of Precipitation in Eastern Hungary: Implications on Isotope Hydrology and Regional Palaeoclimatology. *J. Hydrol.* **2011**, *400*, 144–153. [CrossRef]
25. Vreča, P.; Bronić, I.K.; Horvatinčić, N.; Barešić, J. Isotopic Characteristics of Precipitation in Slovenia and Croatia: Comparison of Continental and Maritime Stations. *J. Hydrol.* **2006**, *330*, 457–469. [CrossRef]
26. Borković, D.; Kovač, Z.; Krajcar Bronić, I. Time-Series Analysis of Isotope Composition of Precipitation in Zagreb, Croatia. *Water* **2022**, *14*, 2008. [CrossRef]
27. Bronić, I.K.; Barešić, J.; Borković, D.; Sironić, A.; Mikelić, I.L.; Vreča, P. Long-Term Isotope Records of Precipitation in Zagreb, Croatia. *Water* **2020**, *12*, 226. [CrossRef]
28. Palcsu, L.; Molnár, M.; Major, Z.; Svingor, E.; Veres, M.; Barnabás, I.; Kapitány, S. Detection of Tritium and Alpha Decaying Radionuclides in L/ILW by Measurements of Helium Isotopes. *J. Radioanal. Nucl. Chem.* **2010**, *286*, 483–487. [CrossRef]
29. Papp, L.; Palcsu, L.; Major, Z.; Rinyu, L.; Tóth, I. A Mass Spectrometric Line for Tritium Analysis of Water and Noble Gas Measurements from Different Water Amounts in the Range of Microlitres and Millilitres. *Isot. Environ. Health Stud.* **2012**, *48*, 494–511. [CrossRef]
30. Draxler, R.R.; Hess, G.D. *Description of the HYSPLIT_4 Modeling System*; Report number: NOAA Technical Memorandum ERL ARL-224; NOAA Air Resources Laboratory: Silver Spring, MD, USA, 1997. Available online: https://repository.library.noaa.gov/view/noaa/31133#tabs-4 (accessed on 23 November 2026).
31. Draxler, R.R.; Hess, G.D. An Overview of the HYSPLIT_4 Modelling System for Trajectories, Dispersion, and Deposition. *Aust. Meteorol. Mag.* **1998**, *47*, 295–308. [CrossRef]
32. Stein, A.F.; Draxler, R.R.; Rolph, G.D.; Stunder, B.J.B.; Cohen, M.D.; Ngan, F. NOAA's HYSPLIT Atmospheric Transport and Dispersion Modeling System. *Bull. Am. Meteorol. Soc.* **2015**, *96*, 2059–2077. [CrossRef]
33. Cross, M. Pysplit: A Package for the Generation, Analysis, and Visualizations of Hysplit Air Parcel Trajectories. In Proceedings of the 14th Annual in Scientific Computing with Python Conference (SciPy 15), Austin, TX, USA, 6–12 July 2015.
34. Warner, M.S.C. Introduction to PySPLIT: A Python Toolkit for NOAA ARL's HYSPLIT Model. *Comput. Sci. Eng.* **2018**, *20*, 47–62. [CrossRef]
35. Carslaw, D.C.; Ropkins, K. Openair—An R Package for Air Quality Data Analysis. *Environ. Model. Softw.* **2012**, *27–28*, 52–61. [CrossRef]
36. Bowen, G.J.; Wassenaar, L.I.; Hobson, K.A. Global Application of Stable Hydrogen and Oxygen Isotopes to Wildlife Forensics. *Oecologia* **2005**, *143*, 337–348. [CrossRef]
37. Bowen, G.J.; Revenaugh, J. Interpolating the Isotopic Composition of Modern Meteoric Precipitation. *Water Resour. Res.* **2003**, *39*, 2003WR002086. [CrossRef]
38. Cauquoin, A.; Fourré, É.; Landais, A.; Okazaki, A.; Yoshimura, K. Cosmogenic Tritium Data Model. By MIROC5-Iso [Dataset]. 2023. Available online: https://zenodo.org/records/10223858 (accessed on 23 November 2026).
39. Yabra, M.S.; de Elía, R.; Vidal, L.; Nicolini, M. Intercomparison Between METAR- and SYNOP-Based Fog Climatologies. *Pure Appl. Geophys.* **2024**, *181*, 1337–1361. [CrossRef]
40. Rozanski, K.; Gonfiantini, R.; Araguas-Araguas, L. Tritium in the Global Atmosphere: Distribution Patterns and Recent Trends. *J. Phys. G Nucl. Part. Phys.* **1991**, *17*, S523–S536. [CrossRef]
41. Rooyen, J.D.; Watson, A.P.; Palcsu, L.; Miller, J.A. Constraining the Spatial Distribution of Tritium in Groundwater Across South Africa. *Water Resour. Res.* **2021**, *57*, e2020WR028985. [CrossRef]
42. Goosse, H. *Climate System Dynamics and Modelling*; Cambridge University Press: Cambridge, UK, 2015.
43. Hurrell, J.W.; Kushnir, Y.; Ottersen, G.; Visbeck, M. An Overview of the North Atlantic Oscillation. *Geophys. Monogr.-Am. Geophys. Union* **2003**, *134*, 1–35. [CrossRef]

44. Pitakchaianan, C.; Kosinarkaranun, K.; Kumsut, P.; Hazama, R.; Rittirong, A.; Sakakibara, K.; Kashiwaya, K.; Ogata, Y.; Kato, Y.; Akata, N.; et al. Tritium Baseline Concentration and the Origins of Water and Solute in Precipitation Elucidated from Monthly Data in Osaka, Japan. *J. Environ. Radioact.* **2026**, *292*, 107878. [CrossRef]
45. Roos, D.V.D.; Schooling, H.; Vogel, J.C.; Triegaardt, D.O. Deuterium in Hailstones Collected on 29 November 1972. *Q. J. R. Meteorol. Soc.* **1977**, *103*, 751–767. [CrossRef]
46. Jouzel, J. Isotopes in Cloud Physics: Multiphase and Multistage Condensation Processes. In *The Terrestrial Environment, B*; Elsevier: Amsterdam, The Netherlands, 1986; pp. 61–112, ISBN 978-0-444-42225-5.
47. Merlivat, L.; Jouzel, J. Global Climatic Interpretation of the Deuterium-Oxygen 18 Relationship for Precipitation. *J. Geophys. Res. Ocean.* **1979**, *84*, 5029–5033. [CrossRef]
48. Jouzel, J.; Merlivat, L.; Roth, E. Isotopic Study of Hail. *J. Geophys. Res.* **1975**, *80*, 5015–5030. [CrossRef]
49. Federer, B.; Brichet, N.; Jouzel, J. Stable Isotopes in Hailstones. Part I: The Isotopic Cloud Model. *J. Atmos. Sci.* **1982**, *39*, 1323–1335. [CrossRef]
50. Miyake, Y.; Matsubaya, O.; Nishihara, C. An Isotopic Study on Meteoric Precipitation. *Pap. Meteorol. Geophys.* **1968**, *19*, 243–266. [CrossRef]
51. Risi, C.; Bony, S.; Vimeux, F. Influence of Convective Processes on the Isotopic Composition (δ^{18} O and δ D) of Precipitation and Water Vapor in the Tropics: 2. Physical Interpretation of the Amount Effect. *J. Geophys. Res.* **2008**, *113*, 2008JD009943. [CrossRef]
52. Ehhalt, D.H. Deuterium and Tritium Content of Hailstones: Additional Information on Their Growth. *Trans. Amer. Geophys. Union Meet.* **1967**, *48*, 106–107.
53. Knight, C.A.; Ehhalt, D.H.; Roper, N.; Knight, N.C. Radial and Tangential Variation of Deuterium in Hailstones. *J. Atmos. Sci.* **1975**, *32*, 1990–2000. [CrossRef]
54. Chang, H.K.; Gonçalves, R.D.; Aggarwal, P.K.; Stradioto, M.R.; Hespanhol, E.C.B.; Sturchio, N.C.; Romatschke, U.; Araguas, L.J.A. Groundwater Isotope Ratios Reflect Convective and Stratiform (Paleo)Precipitation Fractions in Brazil. *J. Hydrol.* **2020**, *585*, 124801. [CrossRef]
55. Landshuter, N.; Aemisegger, F.; Mölg, T. Stable Water Isotope Signals and Their Relation to Stratiform and Convective Precipitation in the Tropical Andes. *JGR Atmos.* **2024**, *129*, e2023JD040630. [CrossRef]
56. Munksgaard, N.C.; Kurita, N.; Sánchez-Murillo, R.; Ahmed, N.; Araguas, L.; Balachew, D.L.; Bird, M.I.; Chakraborty, S.; Kien Chinh, N.; Cobb, K.M.; et al. Data Descriptor: Daily Observations of Stable Isotope Ratios of Rainfall in the Tropics. *Sci. Rep.* **2019**, *9*, 14419. [CrossRef]
57. Bevacqua, C.-F.; Schleussner, E.; Zscheischler, J. A Year above 1.5 °C Signals That Earth Is Most Probably within the 20-Year Period That Will Reach the Paris Agreement Limit. *Nat. Clim. Change* **2025**, *15*, 262–265. [CrossRef]
58. Jouzel, J. Water Stable Isotopes: Atmospheric Composition and Applications in Polar Ice Core Studies. In *Treatise on Geochemistry*; Elsevier: Amsterdam, The Netherlands, 2014; pp. 213–256, ISBN 978-0-08-098300-4.
59. Bowen, G.J. Isoscapes: Spatial Pattern in Isotopic Biogeochemistry. *Annu. Rev. Earth Planet. Sci.* **2010**, *38*, 161–187. [CrossRef]
60. Poluianov, S.V.; Kovaltsov, G.A.; Usoskin, I.G. A New Full 3-D Model of Cosmogenic Tritium3 H Production in the Atmosphere (CRAC:3H). *JGR Atmos.* **2020**, *125*, e2020JD033147. [CrossRef]

Disclaimer/Publisher's Note: The statements, opinions and data contained in all publications are solely those of the individual author(s) and contributor(s) and not of MDPI and/or the editor(s). MDPI and/or the editor(s) disclaim responsibility for any injury to people or property resulting from any ideas, methods, instructions or products referred to in the content.